JOURNAL OF GEOPHYSICAL RESEARCH, VOL. 113, D24118, doi:10.1029/2008JD010561, 2008

Muted precipitation increase in global warming simulations: A surface evaporation perspective

Ingo Richter[1] and Shang-Ping Xie[1,2]

Received 6 June 2008; revised 24 September 2008; accepted 7 November 2008; published 31 December 2008.

[1] Atmospheric moisture content is expected to rise in response to global warming, but climate models predict a much slower rate of precipitation increase. This muted response of the hydrological cycle is investigated from a surface evaporation perspective, using a multimodel ensemble of simulations under the A1B forcing scenario. A 90-year analysis of surface evaporation based on a standard bulk formula reveals that the following atmospheric changes act to slow down the increase in surface evaporation over ice-free oceans: surface relative humidity increases by 1.0%, surface stability, as measured by air-sea temperature difference, increases by 0.2 K, and surface wind speed decreases by 0.02 m/s. As a result of these changes, surface evaporation increases by only 2% per Kelvin of surface warming, rather than the 7%/K rate simulated for atmospheric moisture. The increased surface stability and relative humidity are robust across models. The former is nearly uniform over ice-free oceans while the latter features a subtropical peak on either side of the equator. While relative humidity changes are positive almost everywhere in a thin surface layer, changes aloft show positive trends in the deep tropics and negative ones in the subtropics. The surface-trapped structure suggests the following mechanism: owing to its thermal inertia, the ocean lags behind the atmospheric warming, and this retarding effect causes an increase in surface stability and relative humidity, analogously to advection fog. Our results call for observational efforts to monitor and detect changes in surface relative humidity and stability over the world ocean.

Citation: Richter, I., and S.-P. Xie (2008), Muted precipitation increase in global warming simulations: A surface evaporation perspective, *J. Geophys. Res.*, *113*, D24118, doi:10.1029/2008JD010561.

1. Introduction

[2] One of the important consequences of a rise in global atmospheric temperatures is the increase of the atmosphere's capacity to hold water vapor in accordance with the Clausius-Clapeyron (CC) equation. Under the assumption of constant relative humidity, this implies an increase in specific humidity at the rate of ~7% per Kelvin of atmospheric warming, a prediction roughly borne out by observations and model simulations. If, in addition, the atmospheric circulation remained approximately unchanged, we would expect precipitation to increase at a similar rate as water vapor. This, however, is not what is predicted by a wide array of climate models, which put the rate of precipitation increase at just 2%/K [*Held and Soden*, 2006]. One way the models can achieve this muted precipitation response is through a slowdown of the tropical circulation so that the decrease in upward velocity partially offsets the increase in atmospheric moisture [*Emori and Brown*, 2005]. Such a slow down is confirmed for the simulated Walker Circulation [*Vecchi and Soden*, 2007] and, to a lesser extent, for the Hadley Circulation [*Lu et al.*, 2007].

[3] The muted precipitation increase and slowing of the tropical circulation constitute a consistent response to greenhouse gas (GHG) forcing among models but it is not obvious why the climate system should behave in this particular manner. In fact, recent observational studies by *Wentz et al.* [2007] and *Allan and Soden* [2007] suggest that the actual rate of precipitation increase might be significantly higher than what is simulated by climate models. Similarly, a recent analysis of surface heat flux using merged satellite and reanalysis data [*Yu and Weller*, 2007] indicates a rate of latent heat flux increase that is much higher than in the models. While these observational studies are still subject to measurement errors and natural variability in short data records (see *Lambert et al.* [2008] and *Previdi and Liepert* [2008] for a discussion of the results of Wentz et al.), it is important to achieve a physical understanding of the reasons behind the muted precipitation response in model simulations.

[4] The present study explores the simulated climate changes from a global hydrological cycle perspective. Since global precipitation and surface evaporation are nearly in balance (on monthly and longer timescales), we can address the problem of the muted precipitation increase from either side. Here, we take an evaporation perspective because an

[1]International Pacific Research Center, SOEST, University of Hawaii at Manoa, Honolulu, Hawaii, USA.
[2]Department of Meteorology, University of Hawaii at Manoa, Honolulu, Hawaii, USA.

0148-0227/08/2008JD010561$09.00

analysis of precipitation would have to deal with the complexities of different convection schemes among models. The formulation of surface evaporation, on the other hand, is based on similar bulk formulae with only minor variations across models. Thus we use a standard bulk formula as our starting point, and, by means of decomposition, identify factors crucial to the muted increase of surface evaporation in global warming simulations. It will be shown that both surface relative humidity and air-sea temperature difference do not remain constant but rather exhibit small but robust trends that significantly reduce surface evaporation and thereby slow down the precipitation increase under global warming. *Du and Xie* [2008] used a similar approach to investigate the robust Indian Ocean warming observed during the 20th century. While their study emphasized the regional surface energy balance of the Indian Ocean, the present study is global in scale and focuses on the hydrological cycle under stronger GHG forcing, with an emphasis on surface latent heat flux.

[5] Section 2 introduces the methodology for decomposing the bulk formula of latent heat flux, along with a description of the data used. Section 3 applies this method to latent heat flux changes simulated for the 21st century and identifies the major contributions. Section 4 examines the processes associated with these contributions and identifies surface relative humidity changes as a major player. This motivates an examination of relative humidity changes over the entire troposphere in section 5. Section 6 is a summary and discussion of our results. Details of the latent heat flux decomposition are given in Appendix A, while temperature and moisture contributions to tropospheric relative humidity changes are analyzed in Appendix B.

2. Data and Methods

[6] This study analyzes fully coupled model simulations performed for the Intergovernmental Panel on Climate Change's (IPCC) Fourth Assessment Report (AR4) and archived by the Program for Climate Model Diagnostics and Intercomparison (PCMDI). GHG and aerosol forcing are prescribed according to the IPCC Special Report on Emissions Scenarios (SRES) A1B scenario. This scenario represents a cautiously optimistic estimate of future GHG increases, with CO_2 approximately doubling between 2000 and 2100, after which radiative forcings are held constant. While most model integrations extend for another 100–200 years, our focus is on the period 2000–2100. In some of our analyses, we calculate the 90-year difference between the decadal averages centered on 2005 and 2095. For reasons to be discussed below in this section, the latent heat flux decomposition uses a shorter period (2046–2101). Changes are calculated as the 45-year difference between the first and last decades of this period. Zonal and global averages, unless noted otherwise, are performed for ocean points only.

[7] All of the models consist of an atmospheric general circulation model (GCM) coupled to an oceanic GCM and include land surface models of varying complexity. Models with flux correction schemes are not considered. A list of the models selected for this study is given in Table 1. The ensemble mean shown in Figures 2, 3, 5–10, 12, 13, and B1 refers to the mean over all these models, except for Figures 5 and 6, which show the mean over models for which the decomposition was performed (see footnote "a" in Table 1).

[8] Our analysis of surface latent heat flux changes is based on the standard bulk formula

$$Q_E = L_v C_E \rho_a W (q_s - q_a), \tag{1}$$

where Q_E is latent heat flux, L_v latent heat of evaporation, C_E the transfer coefficient, ρ_a surface air density, W surface wind speed, q_s saturation specific humidity at the sea surface interface, and q_a surface specific humidity. This can be rewritten as

$$Q_E = L_v C_E \rho_a W [q_s(T) - RH \cdot q_s(T + S)], \tag{2}$$

where T is sea surface temperature (SST), $S = T_a - T$, T_a is surface air temperature, and RH is relative humidity. The saturation specific humidity, q_s, is a function of temperature only, according to the CC equation

$$\frac{d \ln e_s}{dT} = \frac{L_v}{R_v T^2}, \tag{3}$$

where e_s is saturation vapor pressure, and R_v is the gas constant for moist air. Integrating (3) one arrives at an analytic expression for e_s [e.g., *Emanuel*, 1994] that yields the following equation for the saturation specific humidity:

$$q_s(T) = q_0 e^{\beta(T)}, \tag{4}$$

where q_0 is a constant and $\beta(T)$ is a function of T. Substituting (4) into (2), we obtain

$$Q_E = L_v C_E \rho_a W q_0 \left(e^{\beta(T)} - RH \cdot e^{\beta(T+S)} \right) \tag{5}$$

and have thus expressed latent heat flux in terms of wind speed, SST, surface stability, and surface relative humidity. Surface latent heat flux changes can be approximated through a Taylor expansion of (5). We illustrate the technique for the SST contribution. The exact expressions along with further details on the technique can be found in Appendix A.

[9] If we assume, for the moment, that $\beta(T) = \alpha T$, where α is a constant, then the partial derivative of (5) with respect to T is $\frac{\partial Q_E}{\partial T} = \alpha Q_E$. The SST contribution may then be expressed as $\alpha Q_E^0 T'$, where Q_E^0 is latent heat flux of the reference state. This represents a restoring term that is linear in T' and will thus be called Newtonian cooling. Note that, more generally, Newtonian cooling usually denotes a restoring term that incorporates the effects of sensible, latent, and radiative surface fluxes, while in our definition it represents only a component of latent heat flux. In the actual computations, we use a more accurate expression for β, namely

$$\beta(T) = \exp(a - b/T - c \ln T), \tag{6}$$

where a, b, and c are constants.

[10] Besides Newtonian cooling other major contributions to latent heat flux changes come from surface relative

Table 1. List of the Models Considered in This Study

Model	Modeling Center
BCCR BCM 2.0[a]	Bjerknes Centre for Climate Research, Norway
CNRM CM 3[a]	Centre National de Recherches Meterologiques, France
CSIRO Mk 3.5[a]	Commonwealth Scientific and Industrial Research Organization, Australia
GFDL CM 0[a]	Geophysical Fluid Dynamics Laboratory, USA
GFDL CM 1[a]	Geophysical Fluid Dynamics Laboratory, USA
GISS Model ER[a]	NASA Goddard Institute for Space Studies, USA
IAP FGOALS g1.0[a]	LASG Institute of Atmospheric Physics, China
INGV ECHAM4	Instituto Nazionale di Geofisica e Vulcanologia, Italy
INMCM 3.0[a]	Institute for Numerical Mathematics, Russia
IPSL CM 4[a]	Institut Pierre-Simon Laplace, France
MIROC 3.2 (high resolution)[a]	Center for Climate System Research (CCSR), Japan
MIROC 3.2 (low resolution)[a]	Center for Climate System Research (CCSR), Japan
MPI ECHAM 5[a]	Max Planck Institute for Meteorology, Germany
NCAR CCSM 3.0	National Center for Atmospheric Research, USA
NCAR PCM 1	National Center for Atmospheric Research, USA
UKMO HadGEM 1	Met Office Hadley Centre for Climate Prediction, UK

[a]Used for the detailed latent heat flux analysis.

humidity, stability, and wind speed. Since the Newtonian cooling term depends on SST changes only, it can be interpreted as representing the oceanic response to latent heat flux changes. By itself, this term would mandate an increase of surface evaporation at the CC rate. The other three terms, on the other hand, constitute atmospheric adjustments that modify the actual latent heat flux. The wind speed and Newtonian cooling terms interact in the tropics, a feature known as the wind-evaporation-SST (WES) feedback, which has been studied extensively in the context of the northward displacement of the intertropical convergence zone (ITCZ) [*Xie*, 2004] and meridional mode of tropical variability [*Chang et al.*, 2006].

[11] A major benefit of our decomposition technique is to separate the evaporation response to global warming into oceanic and atmospheric terms. While the oceanic term (Newtonian cooling) represents an increase of evaporation at the CC rate, the atmospheric terms oppose this, as will be shown in section 3. Thus our decomposition provides a convenient framework to analyze the factors controlling the evaporation/precipitation response. Moreover, the atmospheric response is cast in terms of quantities that are of general meteorological and climatological interest and are routinely measured. Of particular interest are potential changes in relative humidity as many observational [*Wentz and Schabel*, 2000; *Trenberth et al.*, 2005; *Soden et al.*, 2005; *Dai*, 2006; *Willett et al.*, 2007] and modeling studies [e.g., *Cess et al.*, 1990; *Held and Soden*, 2000; *Ingram*, 2002] report that this quantity remains almost unchanged under global warming. This might imply that changes of relative humidity under global warming are inconsequential. The present study, however, demonstrates that relative humidity does change significantly under GHG forcing, and that, at the surface, these changes strongly influence the hydrological cycle.

[12] In the AR4 archive, SST is directly available, and the air-sea temperature difference is readily calculated from surface air temperature. Relative humidity is not available as a surface quantity, and was therefore calculated from monthly mean surface specific humidity and temperature. Using monthly means might incur some errors due to the nonlinear dependence of relative humidity on temperature and specific humidity, particularly in the midlatitudes where synoptic variability is pronounced. Our results from an alternative derivation using daily temperature and humidity values indicate that these errors are small.

[13] Scalar surface wind speed is not available in the IPCC database and is therefore calculated from the zonal and meridional components. To increase accuracy, this is done by using daily rather than monthly means. The use of daily output limits our latent heat flux decomposition to a shorter period, 2046–2101.

[14] For some of the AR4 models not all the variables necessary for the calculation were available. The models for which the decomposition was performed are marked by footnote "a" in Table 1.

3. Latent Heat Flux Changes

[15] We start by verifying the correspondence between precipitation and surface evaporation in the AR4 simulations. Figure 1 examines the temporal correlation between global monthly mean precipitation and evaporation anomalies (land points included) for the period 2040–2045. Evaporation tracks precipitation very well with correlations ranging from 92% to 95% among models. When a 7-month running mean is applied, correlations increase to 98–99%. Some degree of atmospheric storage is noticeable as both positive and negative evaporation anomalies exceed those of precipitation. This storage must have a positive trend because atmospheric water vapor increases over time. To estimate the importance of the storage trend we calculated the precipitation minus evaporation (PME) difference for the period 2000–2100. The trend is approximately 0.2% of the precipitation increase and thus negligibly small for our purposes. Evaporation can therefore explain precipitation changes and is adequate for analyzing long-term trends.

3.1. Zonal Mean Evaporation Changes

[16] Figure 2a shows the latitudinal distribution of zonal mean precipitation and evaporation (normalized by the global mean increase in surface air temperature) over ocean points. The precipitation increase is 1.8%/K in the global and ensemble mean but displays large meridional variations. The changes in precipitation (Figure 2a) feature a pronounced peak around the equator and a subtropical minimum on either side of the equator that is negative in most models. In contrast, evaporation changes are distributed more evenly and tend to peak at about 10° north and south of the equator. The equatorial dip in evaporation is most pronounced over the western Pacific warm pool, with most models featuring an absolute decrease (not shown). This meridional structure of evaporation and precipitation changes implies increased moisture transport by the surface trades toward the equator resulting in more intense precipitation there.

[17] Also shown in Figure 2a is the difference between relative changes in precipitable water and precipitation. Precipitable water increases significantly faster than precip-

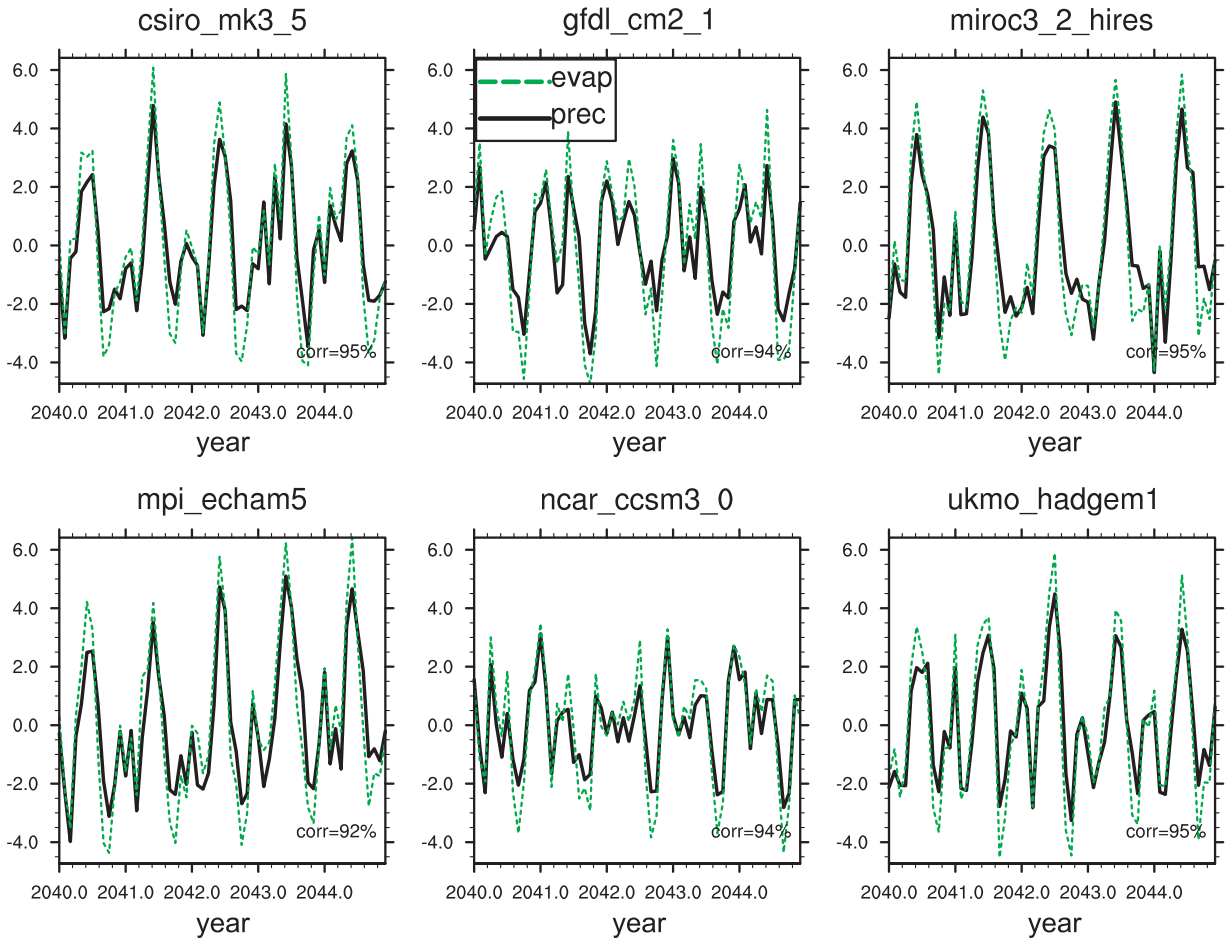

Figure 1. Globally averaged precipitation changes (%, solid black line) and evaporation (%, dashed green line) for the period 2040–2045. Changes are relative to the mean over 2040–2045. The correlation between the two fields is indicated in the lower right.

itation at almost all latitudes, even around the equator where the precipitation trend exceeds 7%/K. This supports the notion that upward motion in deep convective regions must become less intense [*Held and Soden*, 2006] or less frequent [*Trenberth et al.*, 2003].

[18] Over land (Figure 2b), the increase in precipitation is significantly lower than over the ocean, with a global mean increase of only 0.58% in the ensemble mean (some models even feature a precipitation decrease over land). All models still exhibit a peak on the equator, but it is far less pronounced than over the oceans. Changes of evaporation and precipitation are highly correlated over land, suggesting a high recycling rate and little contribution from moisture transport.

3.2. Land Versus Ocean Contributions

[19] To get a sense for the relative importance of ocean and land to the evaporation changes, we show zonally summed land and ocean contributions for the period 2000–2100 (Figure 3). The amplitude of the changes is typically 1 order of magnitude larger over oceans than over land. Moreover, the changes over land are negative at many latitudes for the majority of models so that the increase of global evaporation is dominated by changes over oceans. For this reason, the rest of the paper focuses on oceanic evaporation changes and the factors controlling them.

3.3. Latent Heat Flux Decomposition

[20] The results of the latent heat flux decomposition for the global oceans are shown in Figure 4. The largest contribution comes from the Newtonian cooling term, which is a function of SST warming only and closely follows the CC rate. All other terms are negative (with the exception of the GFDL CM 2.1 and IAP FGOALS wind speed terms), opposing the increase of latent heat flux at the CC rate. As a result, the actual evaporation increase is only a fraction (~30–50%) of the CC prediction. The largest negative contribution in many models comes from the relative humidity term, which, in the ensemble mean, is -1.4 W m^{-2} or about $-1/4$ of the Newtonian cooling term. Assuming a mean relative humidity of 80% and latent heat flux of 100 W m^{-2}, values quite typical of the tropical oceans, the relative humidity increase implied is 0.3%. This is similar to the actual ensemble mean trend of 0.4% for the 45-year period. Thus a small increase in surface relative humidity can have a considerable impact on latent heat flux.

[21] Of similar importance is the air-sea temperature difference. Over most parts of the global ocean, SSTs are

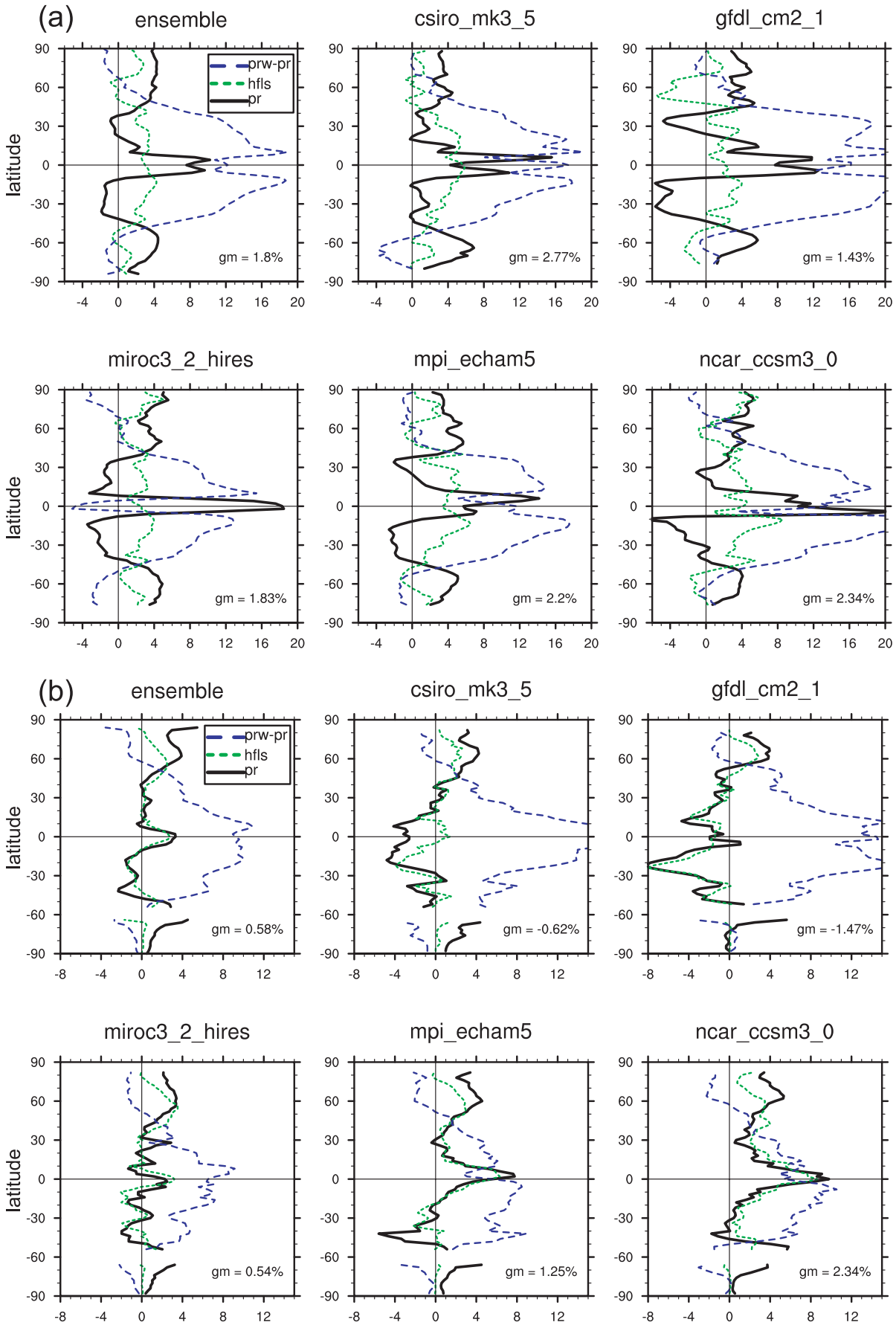
(a)
ensemble
csiro_mk3_5
gfdl_cm2_1
miroc3_2_hires
mpi_echam5
ncar_ccsm3_0
prw-pr
hfls
pr
latitude
gm = 1.8%
gm = 2.77%
gm = 1.43%
gm = 1.83%
gm = 2.2%
gm = 2.34%
(b)
ensemble
csiro_mk3_5
gfdl_cm2_1
miroc3_2_hires
mpi_echam5
ncar_ccsm3_0
prw-pr
hfls
pr
latitude
gm = 0.58%
gm = -0.62%
gm = -1.47%
gm = 0.54%
gm = 1.25%
gm = 2.34%

Figure 2

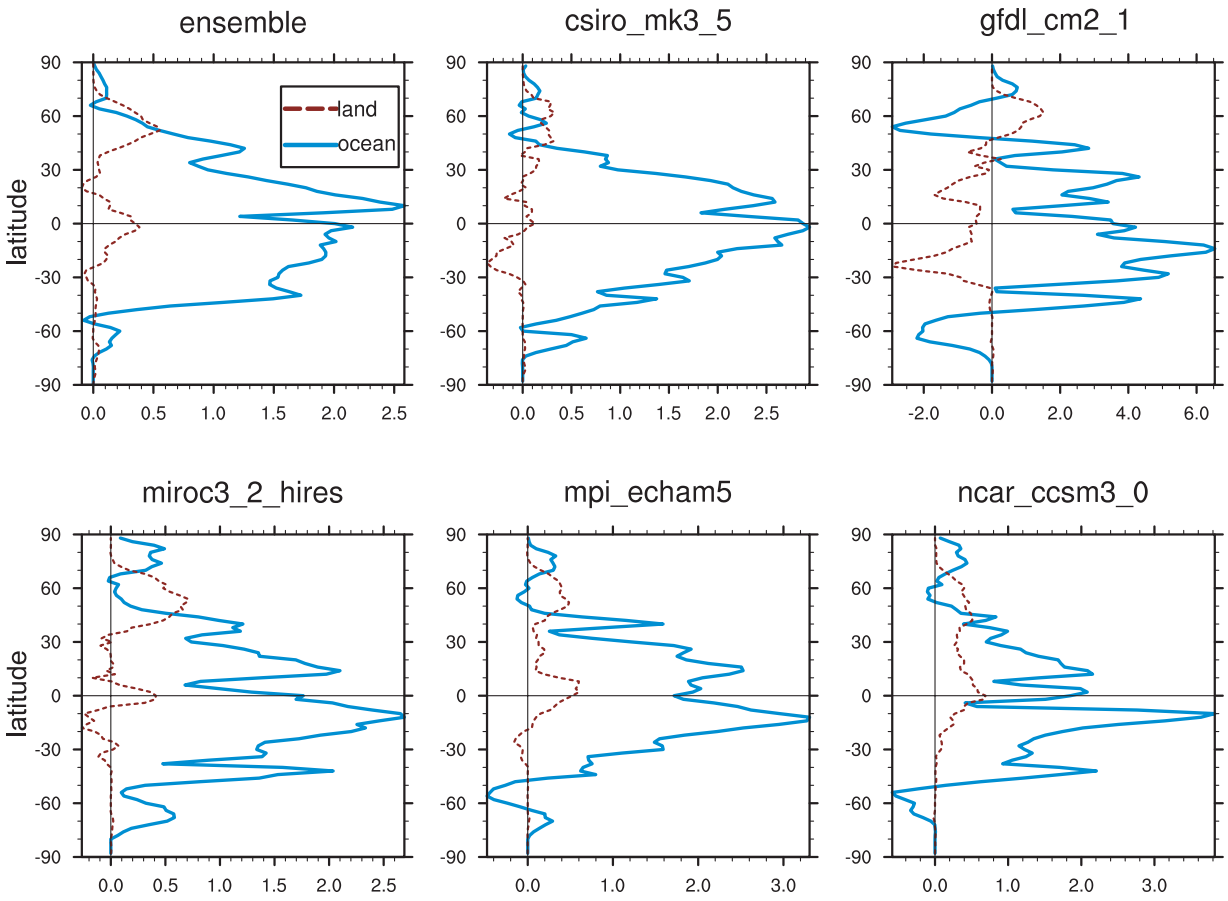

Figure 3. Contribution to the 90-year evaporation changes by latitude for ocean points (blue line) and land points (dashed red line). The fields have been area-weighted and summed by latitude. Units are mm d^{-1}.

higher than the overlying air temperature so that S, as defined in section 2, is negative. Under GHG forcing, the simulated SST increases more slowly than surface air temperature, which increases surface stability. This acts to suppress latent heat release from the ocean and appears as a negative term in our decomposition.

[22] The increased surface stability is consistent with the high heat capacity of the ocean as described in the following. The GHG forcing warms the atmosphere, which acts on the ocean through changes in surface fluxes. The coupled adjustment of the ocean mixed layer and atmosphere takes a few years while thermodynamic adjustment of the deep ocean takes centuries [*Broecker*, 1991]. As heat is transported out of the mixed layer to warm the deeper ocean [e.g., *Gregory*, 2000; *Levitus et al.*, 2005], the upper ocean warming lags that of the atmosphere.

[23] Surface wind speed forms another contribution to the muted latent heat flux response, which is typically smaller than the two other contributions discussed above. In most models, the sign of this term is negative, which is consistent with the slowdown of the tropical circulation as reported by *Vecchi and Soden* [2007] and *Lu et al.* [2007].

3.4. Discussion of the Residuals in the Flux Decomposition

[24] The sum of all contributions is shown as ΔQ_E^{calc} in the bar graph (Figure 4) and juxtaposed to the actual change in latent heat flux (ΔQ_E^{act}). The decomposition is quite successful, with the residuals much smaller than the actual fluxes. An exception to this is the IPA FGOALS model, for which the residual is more than 50% of the actual flux change. The sign of the residual is negative in two models (MIROC 3.2 high resolution and GISS ER) and positive in the others. Possible reasons for the residuals are discussed in Appendix A.

[25] As another measure of how well our decomposition captures actual latent heat flux variations, we show the

Figure 2. Relative changes (% K^{-1}) between 2000 and 2100 (90-year period), normalized by global mean surface air temperature change and plotted as a function of latitude for precipitation (solid black line), evaporation (dotted green line), and precipitable water minus precipitation (dashed blue line). Zonal and global averages were calculated for (a) ocean points only and (b) land points only. The global mean precipitation change is displayed in the bottom right corner of each panel.

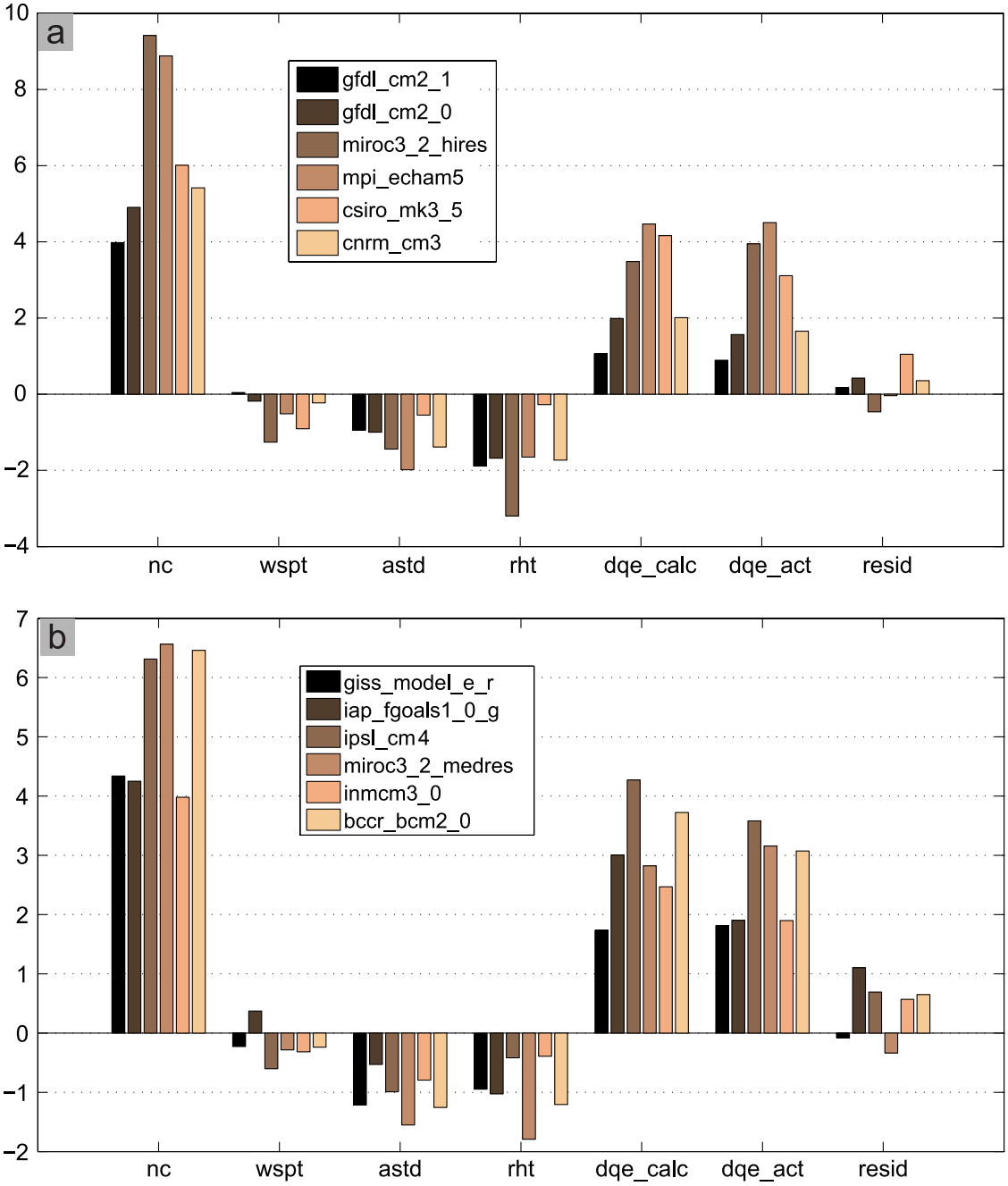

Figure 4. Decomposition of the bulk formula for latent heat flux into the following terms: Newtonian cooling (nc), surface wind speed (wspt), air-sea temperature difference (astd), and surface relative humidity (rht). Also shown are the sum of the decomposition terms (dqe_calc), the actual change in latent heat flux (dqe_act), and the residual (resid) defined as the difference between dqe_act and dqe_calc. The units of the y axis are W m^{-2}. Color shades indicate different models. The analysis period is 2046–2101.

temporal correlation between ΔQ_E^{calc} and ΔQ_E^{act} in Figure 5 (land areas have been masked out). The decomposition works best in the tropical and subtropical regions with correlations typically above 90%, except slightly lower values over the western Pacific warm pool. In the midlatitudes, values drop slightly, sometimes below 80%, suggestive of the importance of synoptic variability. The decomposition works best for the high-resolution MIROC model, for which the correlations between actual and reconstructed evaporation are above 0.9 almost everywhere over the global ocean.

3.5. Meridional Structure of the Decomposition Terms

[26] We further analyze the latent heat flux decomposition by plotting zonal averages of the three major terms (Figure 6). The relative humidity term shows two minima of roughly equal amplitude at about 20°S and 20°N. The

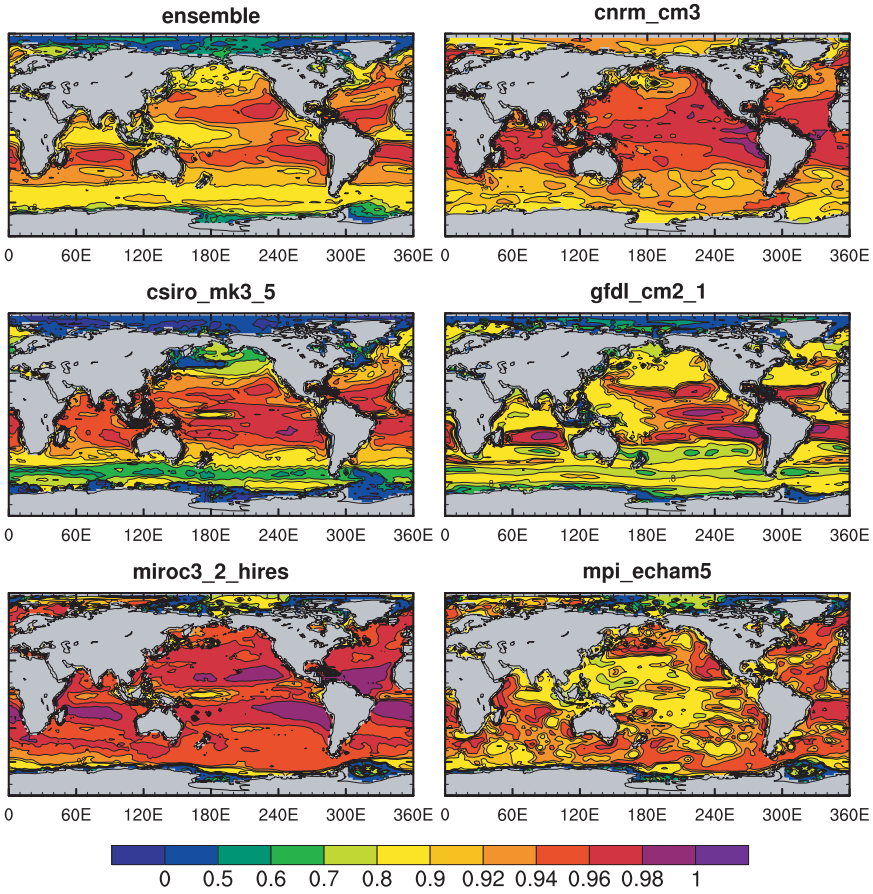

Figure 5. Correlation of latent heat flux changes derived from bulk formula (see text) and the actual latent heat flux change. The correlation between the two quantities is calculated at each grid point for the years 2046–2101. High correlation is found almost everywhere between 30°S and 30°N. Note the nonlinear scale.

wind speed term, on the other hand, tends to be asymmetric about the equator with a maximum in the southern subtropics and a minimum in the northern subtropics. The positive values of the wind speed term in the southern hemisphere partially cancel out negative values elsewhere. Thus, while the wind contribution is quite large at many latitudes, its global mean is rather small. The relative humidity and air-sea temperature difference terms, on the other hand, are negative at almost all latitudes.

[27] With respect to intermodel differences, relative humidity shows the most robust behavior in the tropics and subtropics. The wind speed term is fairly consistent across models in the southern hemisphere but varies considerably in the northern hemisphere. The CSIRO model deviates from all the other models analyzed here in that the relative humidity term is small and that the wind speed term is negative throughout 50°S–40°N.

4. Factors Limiting the Evaporation Increase

[28] Following the result that surface relative humidity, air-sea temperature difference, and wind speed are the major contributors to the muted latent heat flux increase under global warming, this section examines each of these fields in more detail.

4.1. Wind Speed

[29] The most prominent feature of the wind speed changes is the intensification of the westerlies over the Southern Ocean (Figure 7), which is discussed in several papers [*Kushner et al.*, 2001; *Yin*, 2005; *Fyfe and Saenko*, 2005] and supported by observations [*Thompson and Solomon*, 2002; *Yang et al.*, 2007]. This intensification has been linked to GHG forcing as well as changes in the Antarctic polar vortex and the decrease of stratospheric ozone [*Gillett and Thompson*, 2003; *Yang et al.*, 2007; *Deser and Phillips*, 2008]. The associated angular momentum increase is partially balanced by the intensification of the southeast trades, another fairly robust feature in the simulations.

[30] The simulated SST increase is relatively small in the Southern Ocean because its mixed layer is deep and the surface westerlies produce upwelling along the Antarctic continent. This enhances the equatorward gradient of SST and, consequently, that of sea level pressure (SLP; not shown). The intensification of the southern trades is consistent with this SLP pattern.

[31] Another robust feature is the wind speed decrease over the western equatorial Pacific as the Walker circulation weakens [*Vecchi and Soden*, 2007], which, for most models, results in a decrease in surface evaporation. Most models

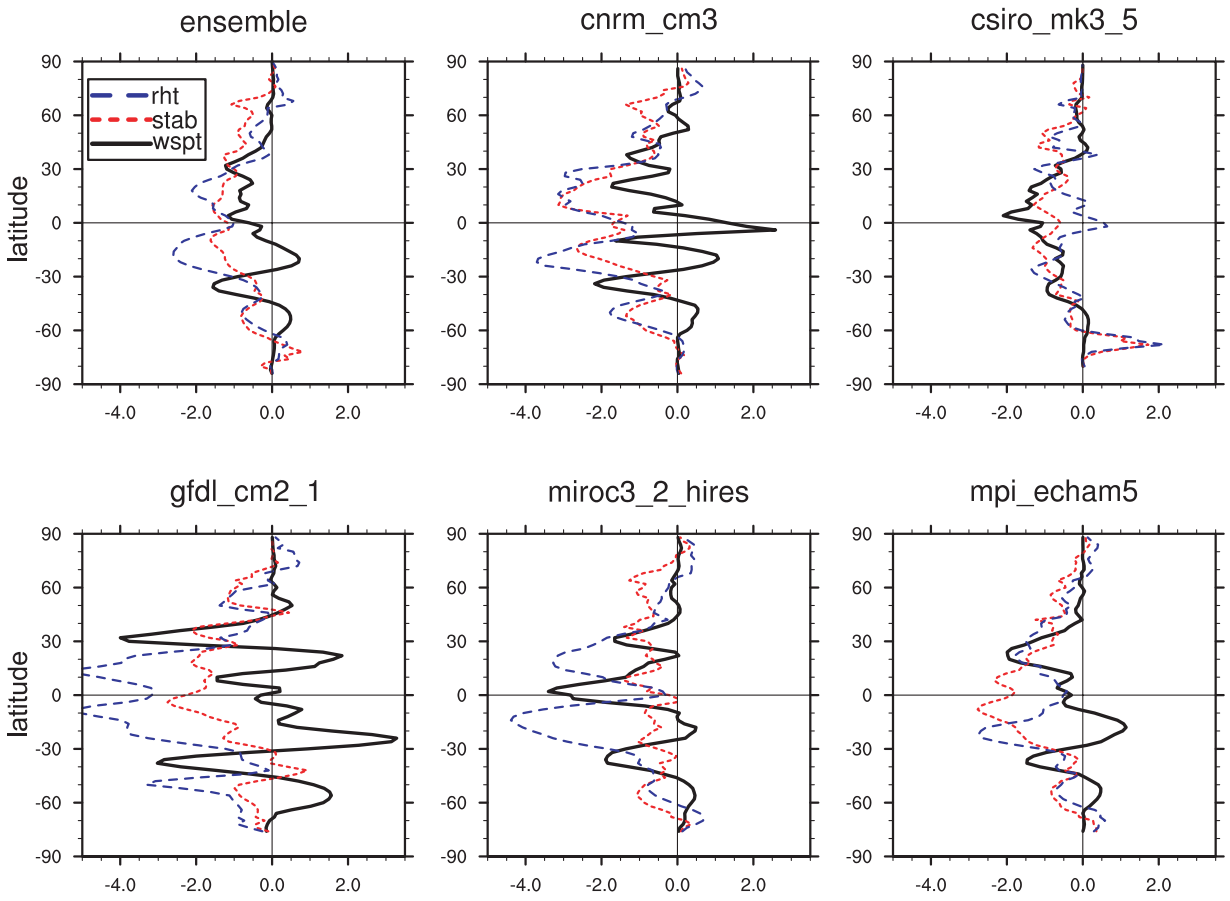

Figure 6. Zonal mean of terms in the latent heat flux decomposition (W m^{-2} K^{-1}) normalized by global mean surface air temperature change. Both zonal and global means are calculated for ocean points only. The individual lines indicate contributions from wind speed (solid black line), air-sea temperature difference (dotted red line), and relative humidity (dashed blue line). Note the anticorrelation of the wind speed and relative humidity terms between 30°S and the equator. The analysis period is 2046–2101.

also show a weakening of the northeast trades over the Pacific, resulting in a north-south asymmetry in wind speed changes that is most apparent in the MIROC high-resolution model. As a result of the opposing trends north and south of the equator, there is only a slight decrease in surface wind speed in the global average.

4.2. Air-Sea Temperature Difference

[32] The difference between surface air temperature and SST (SAT-SST) shows a robust increase over ice-free oceans, with a meridional pattern consistent among all models (Figure 8). The increase in SAT-SST is rather uniform between 30°S and 30°N with a value of about +0.1 K, indicating a stabilization of the near-surface atmosphere. Further poleward, the SAT-SST difference increases to 0.2 K at 60°S and 60°N and then drops to negative values. The former increase may be due to intensified Ekman upwelling that brings prewarming water to the surface while the latter decrease is likely related to changes in sea ice cover.

[33] The robust increase in surface stability (SAT-SST difference) within 60°S–60°N is likely due to the high heat capacity of the ocean, which retards its warming in response to GHG forcing. From an oceanic perspective, the muted latent heat flux response could thus be viewed as a result of the ocean's ability to store heat below the surface.

4.3. Relative Humidity

[34] Surface relative humidity over oceans increases with a subtropical peak of about 1.2% on either side of the equator (Figure 8). There is a local minimum of about 0.6% on the equator (Figure 8), with an absolute decrease over the eastern Pacific cold tongue in most models (not shown). These features are closely tracked by the buoyancy term of the bulk Richardson number, $\frac{g\Delta\theta_v}{T_v\Delta z}$. Here g is the gravitational constant, T_v is virtual temperature, and $\Delta\theta_v$ is the virtual potential temperature difference over a layer of thickness Δz, which, for our calculations, is taken to be 1000–925 hPa. The close relationship of this stability measure with surface relative humidity suggests that the stabilization of the subtropical planetary boundary layer (PBL) under GHG forcing leads to a decrease in PBL ventilation and an increase in surface relative humidity.

[35] The CSIRO MK 3.5 is the only model in which relative humidity remains almost unchanged with a slight decrease around the equator. It is not clear why this model behaves so differently but its PBL parameterization likely plays a role. In the CSIRO MK 3.5, the PBL is parameter-

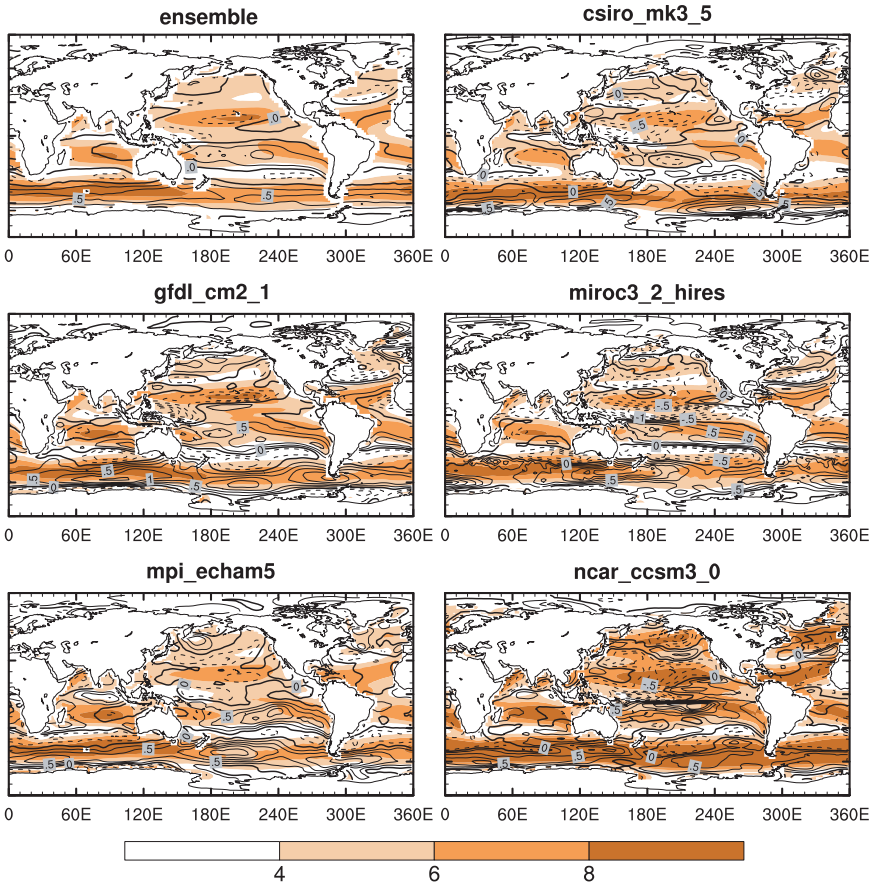

Figure 7. Change in surface wind speed between the periods 2000–2010 and 2090–2100 (m s^{-1}, contours), and the 2000–2010 average (m s^{-1}, color shading). There is a robust acceleration of the westerlies over the Southern Ocean. The southeasterly trades intensify while the northeasterly trades mostly weaken.

ized on the basis of work by *Louis* [1979]. This parameterization also forms the basis of the IPSL and CNRM models, which feature significant surface relative humidity changes. What might set the CSIRO model apart is its parameterization of PBL clouds based on work by *Smith* [1990], which includes the effects of PBL condensation on surface fluxes via the definition of the bulk Richardson number. Also potentially important is the treatment of PBL top entrainment, but this is not documented in the current model description [*Gordon et al.*, 2002].

[36] The combined response of surface stability and relative humidity can be compared to the formation of advection fog. The increase in surface stability means that air temperature warms relative to the sea surface. This is analogous to warm air moving over cold SSTs, a process that increases surface relative humidity. Indeed, if surface relative humidity does increase in nature, we expect marine fog to increase. Whether such a response exists in the models will depend on their PBL formulation.

5. Tropospheric Relative Humidity Changes

5.1. Three-Dimensional Structure

[37] Tropospheric relative humidity affects the water-vapor feedback [*Pierrehumbert*, 1995; *Spencer and Braswell*, 1997; *Sherwood et al.*, 2006] and is closely related to cloud incidence [*Soden and Bretherton*, 1993; *Peixoto and Oort*, 1996; *Sandor et al.*, 2000]. Motivated by the consistent increase in surface relative humidity we examine whether these changes continue aloft. Latitude-height sections of zonal mean relative humidity changes (RH') over the ocean (Figure 9) show that in the subtropics the surface increase is actually confined below the 925-hPa level. With a conservative estimate of 100 hPa for PBL thickness this would mean that relative humidity increases are confined below the PBL top, and possibly also below cloud base. Thus one might expect stratocumulus incidence to decrease under global warming, which is true for the MIROC models (M. Kimoto, personal communication) and probably several others.

[38] The shallowness of the relative humidity increase is further illustrated by vertical profiles averaged between 40°S and 20°S (Figure 10). It is consistent with surface cooling by the ocean.

[39] The general pattern of RH' features an equatorial midtropospheric maximum at about 500 hPa that is flanked by negative trends both in the meridional and vertical directions. The value of the maximum ranges from 3% in the CSIRO Mk 3.5 to 10% in the MIROC high-resolution run, while the subtropical minima range between −2% and −5%. The pattern of tropical increase and subtropical decrease appears to be related to changes in the tropical

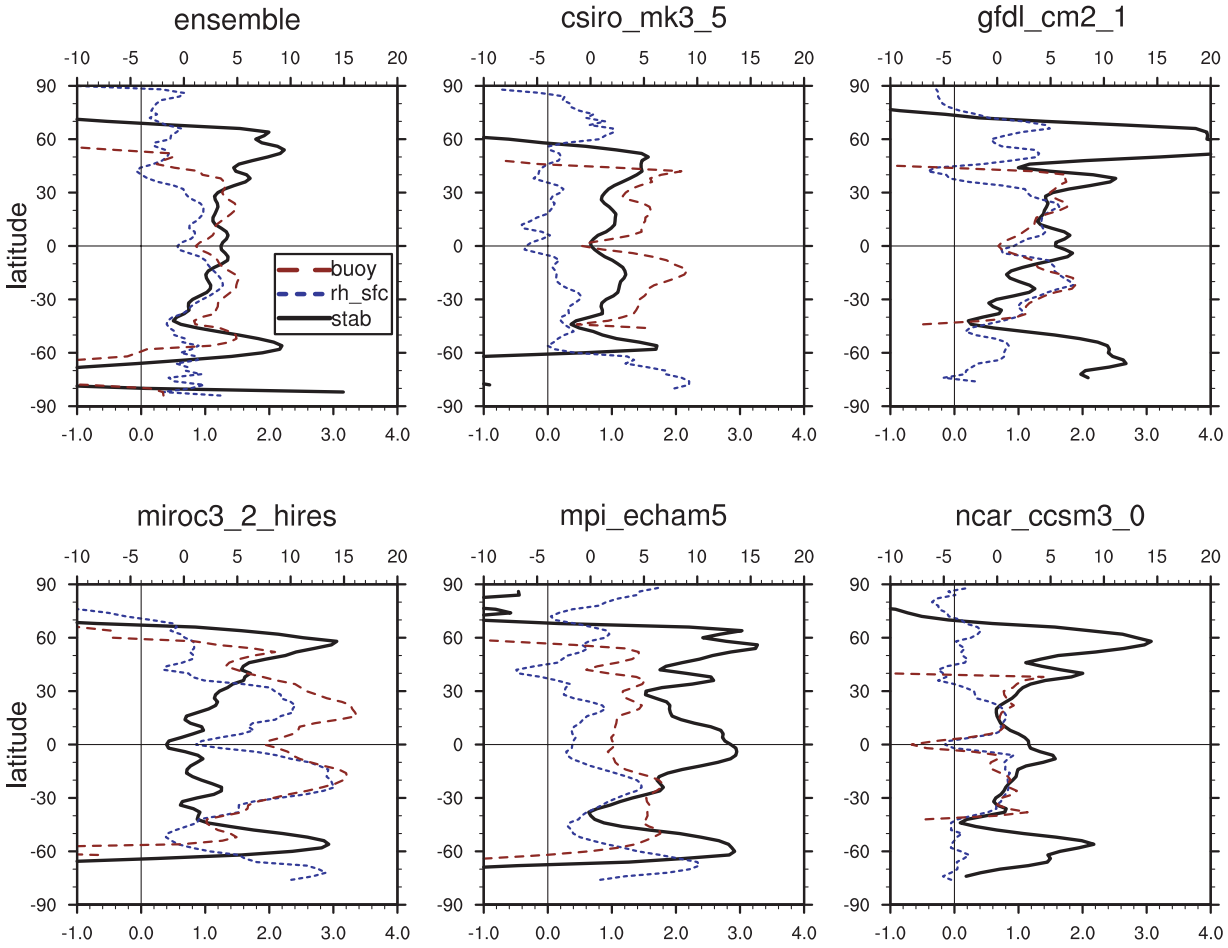

Figure 8. Changes in air-sea temperature difference (K × 0.1, solid black line), surface relative humidity (%, dotted blue line), and the buoyancy term of the bulk Richardson number between 1000 and 925 hPa (s^{-2} × 5.0E5, dashed red line) between the periods 2000–2010 and 2090–2100 for ocean points only.

circulation. This relation with the vertical motion field is substantiated by the horizontal maps of 500 hPa vertical velocity and relative humidity changes (Figure 11), which show that the two fields are highly correlated. A fairly high degree of correspondence between relative humidity and vertical velocity changes also exists in their seasonal evolution (not shown).

[40] RH' is negative in the equatorial upper troposphere between 400 and 150 hPa but positive above (Figure 9). The latter is likely a consequence of the increased tropopause height under global warming [*Lu et al.*, 2007], a feature validated by observations [*Santer et al.*, 2003]. The GFDL CM 2.1 is somewhat different in this regard, because it features a positive RH' between 250 and 150 hPa. This is due to the fact that its temperature increase at those levels is small compared to other models, while its specific humidity increase is about average.

[41] Relative humidity also increases in the lower troposphere poleward of 60° in both hemispheres, but this increase is not as strong as the mid and upper tropospheric maxima. Overall, relative humidity changes in the free tropospheric are more pronounced than in the PBL.

5.2. Changes in Other Relevant Fields

[42] It is instructive to relate the changes in relative humidity with changes in other variables. Figure 12 shows zonally averaged ensemble-mean changes in temperature, specific humidity, and pressure velocity. The largest temperature increase (T') is centered on the equator at about 250 hPa and extends from about 30°S to 30°N (Figure 12a). This peak results from the fact that the tropical atmosphere tends to maintain a moist adiabatic lapse rate [*Xu and Emanuel*, 1989], even under global warming [*Santer et al.*, 2005]. As the moist adiabatic lapse rate decreases with increasing surface temperatures and humidity, a maximum in the upper troposphere arises. This positive temperature trend explains the relative humidity decrease in the upper troposphere (Figure 9).

[43] In the lower troposphere, T' is asymmetric about the equator with high positive values in the northern polar latitudes and comparatively low (but still positive) values in the southern polar latitudes. Negative values of T' are located in the extratropical upper troposphere and stratosphere, probably associated with the increased tropopause

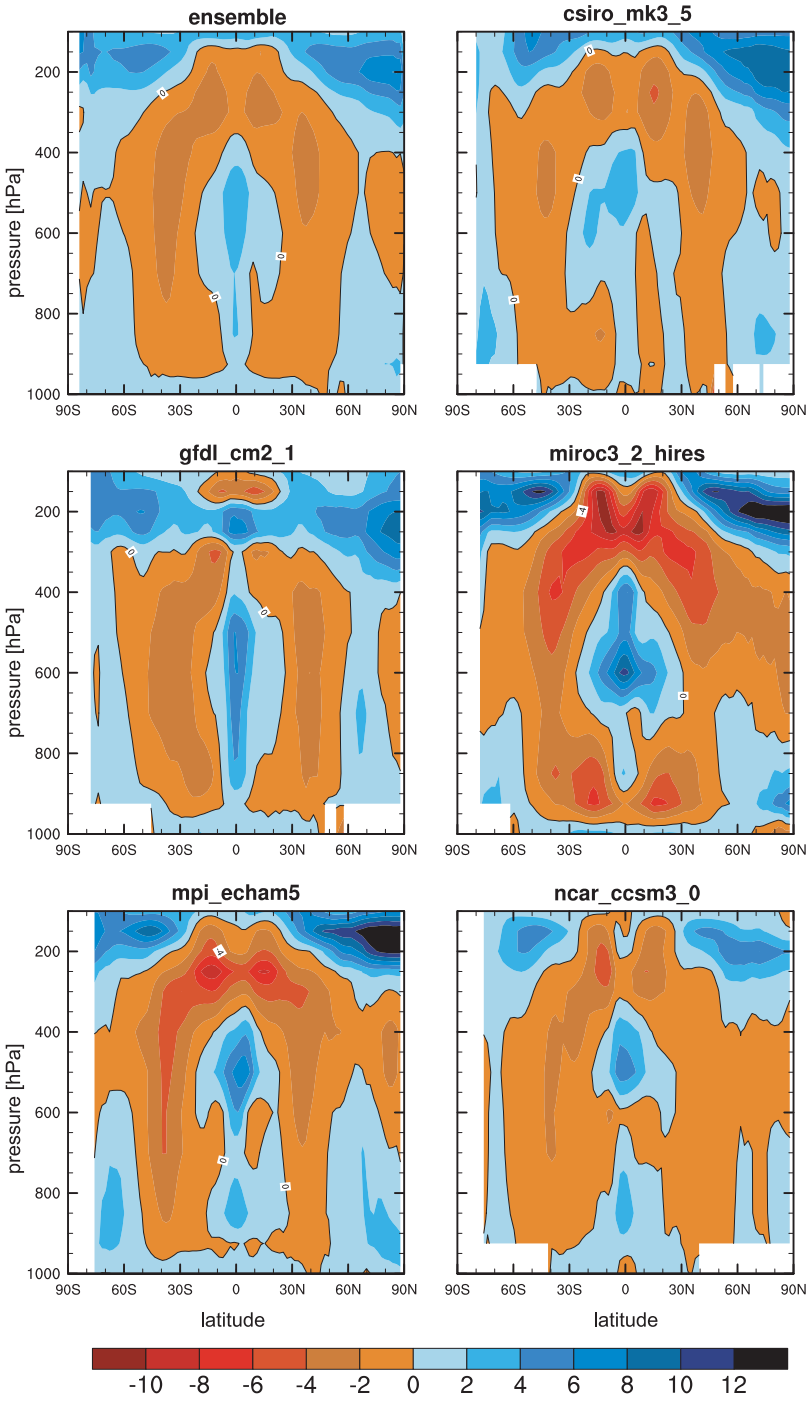

Figure 9. Latitude-height sections of zonal mean relative humidity changes (%) between 2000 and 2100 (ocean points only). Positive and negative values are shaded blue and red, respectively. Areas of increased and decreased relative humidity are associated with major convection and subsidence regions, respectively.

height and increased GHG radiative cooling in the stratosphere.

[44] The specific humidity change (q'; Figure 12b) is positive everywhere and increases from higher latitudes toward the equator and from the upper troposphere toward the surface. This is due to the nonlinearity of the CC equation: as q_s increases approximately exponentially with mean temperature, so does the increase of q_s for a given temperature change. Because q' approximately follows the change in q_s, its maximum is found at equatorial surface levels.

[45] The changes in vertical velocity (Figure 12c) show a rather complex pattern of alternating increases and decreases in the meridional direction. Comparison with

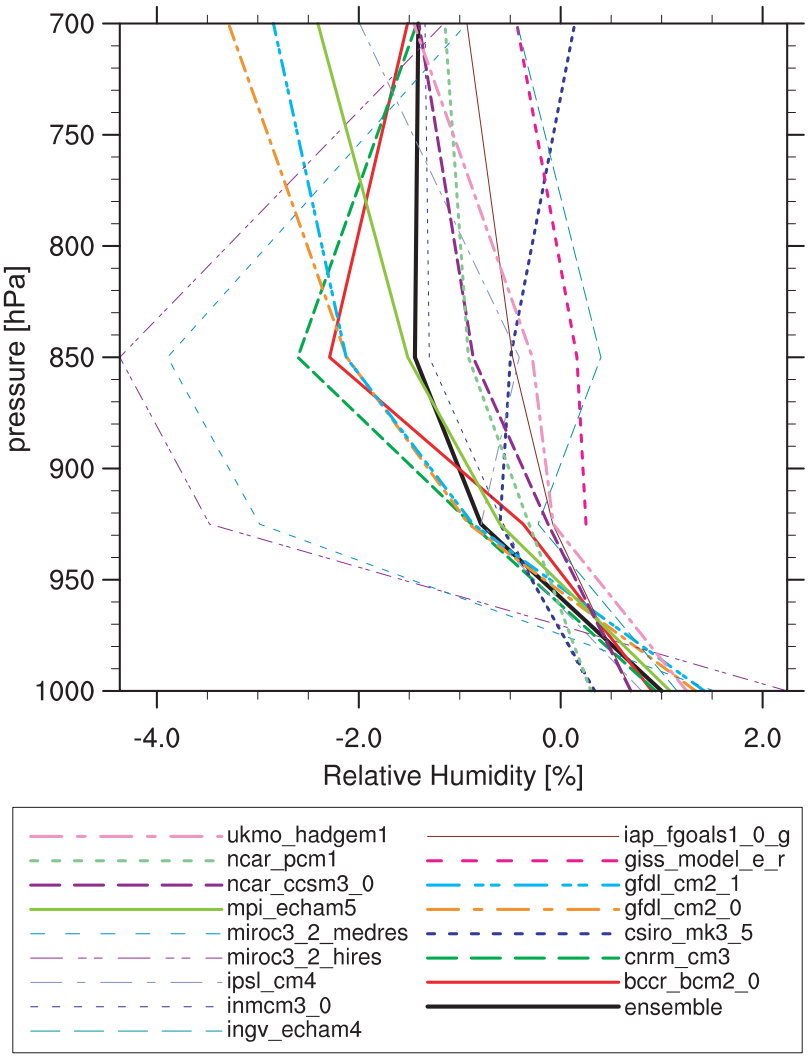

Figure 10. Vertical profiles of lower tropospheric relative humidity changes (%) between 2000 and 2100, averaged between 40°S and 20°S (ocean points only). The solid thick black line represents the ensemble mean.

the mean vertical velocity suggests that tropical convection intensifies at its center (5°S–5°N) but weakens on its flanks, reminiscent of the upped-ante mechanism of *Chou and Neelin* [2004]. Subtropical subsidence, on the other hand, weakens on the equatorward and strengthens on the poleward side, representing a Hadley cell expansion as reported by *Lu et al.* [2007].

5.3. Role of Specific Humidity Advection in Relative Humidity Changes

[46] Relative humidity depends on both specific humidity and temperature but here we focus on the contribution from specific humidity changes. The relative importance of temperature and specific humidity changes is discussed in Appendix B.

[47] Wind velocities may be cast as $w = \bar{w} + w'$, where the basic state ($\bar{w}$) is defined as the mean over the period 2000–2010, and the perturbation (w') is the departure from $\bar{w}$ during the period 2090–2100. We cast specific humidity as $q = \bar{q} + q^{cc} + q^{RH}$, where $\bar{q}$ is the basic state mean, and departures from the mean state are decomposed into two parts: q^{cc} is the change that would result if relative humidity remained constant under global warming, and q^{RH} is the change not explained by q^{cc}, i.e., $q^{RH} = q - \bar{q} - q^{cc}$. Thus a nonzero q^{RH} indicates changes in relative humidity.

[48] Substituting the above decompositions into the vertical advection term ($w\partial q/\partial p$) and neglecting the small nonlinear terms yields

$$(\bar{w} + w') \cdot \frac{\partial}{\partial p}\left(\bar{q} + q^{cc} + q^{RH}\right) = \bar{w}\frac{\partial q^{cc}}{\partial p} + \bar{w}\frac{\partial q^{RH}}{\partial p} + w'\frac{\partial \bar{q}}{\partial p}.$$

[49] Together with the horizontal advection terms derived from $\vec{v}\nabla_p q$ this results in six linear terms of anomalous advection, three of which are shown in zonal mean latitude-height sections in Figures 13a–13c. Their interpretation is given in the following.

[50] The $w'\partial\bar{q}/\partial p$ term (Figure 13a) has a relatively complex meridional structure, similar to the vertical velocity changes (Figure 12c). Close to the equator the positive w' carries more moisture upward leading to a pronounced

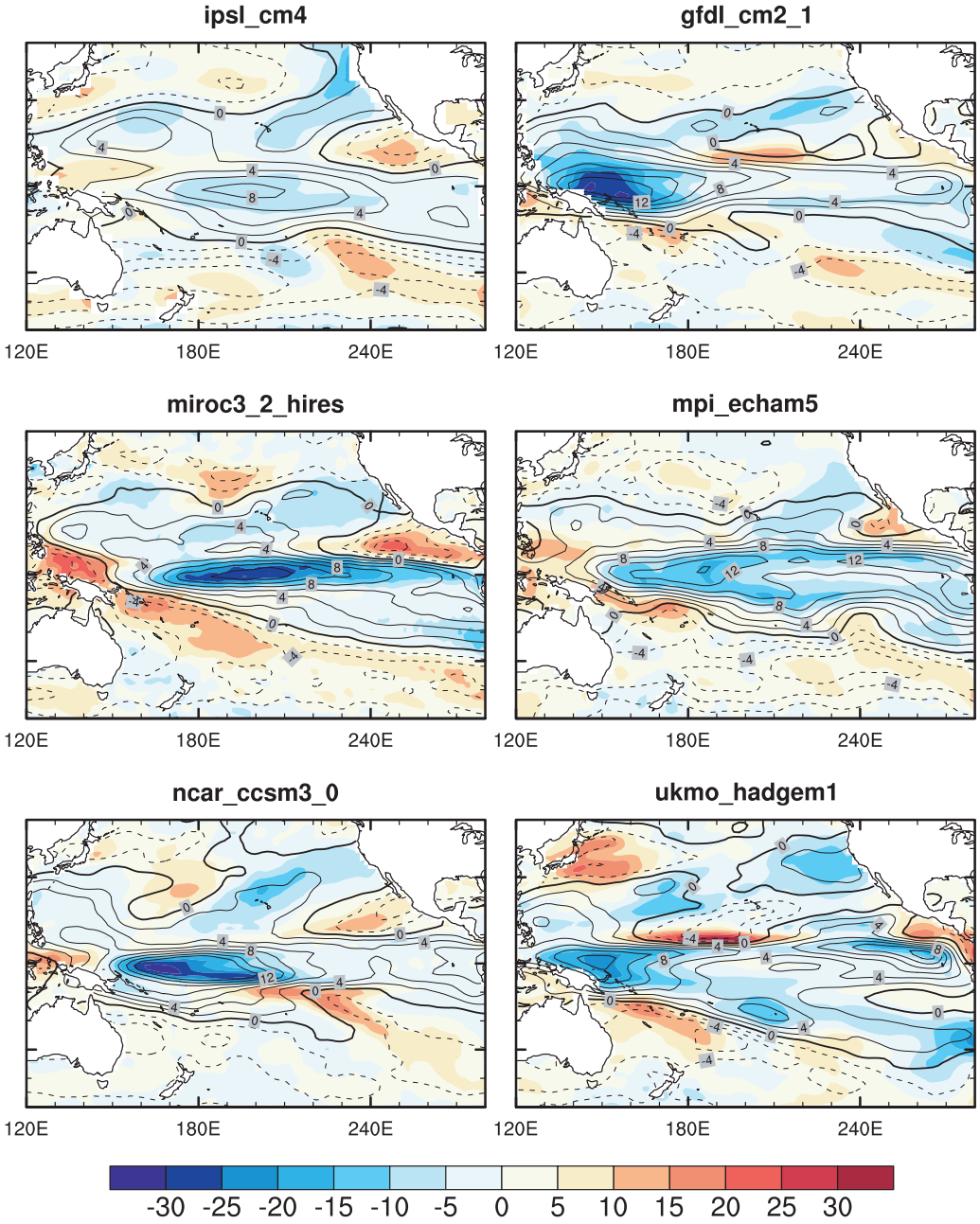

Figure 11. Horizontal maps of changes in relative humidity (%, contours) and vertical pressure velocity (hPa d^{-1}, shading) at 500 hPa. Changes are calculated as the difference between the periods 2000–2010 and 2090–2100. Negative and positive relative humidity changes are indicated by dashed and solid black contour lines, respectively. Blue and red shading denotes negative (upward) and positive (downward) vertical velocity anomalies, respectively.

positive contribution. On the flanks of the deep convective region at 20°S–10°S and 5°N–15°N, the decrease in upward vertical velocity results in a negative contribution from $w'\bar{q}$. This is followed by alternating positive and negative values further poleward in both hemispheres.

[51] The $\bar{w}\partial q^{cc}/\partial p$ term (Figure 13b) displays a simple pattern consistent with the mean vertical motion. Because of the nonlinear CC equation, q^{cc} is dominated by the mean temperature profile and decreases monotonically with height. Thus $\bar{w}\partial q^{cc}/\partial p$ is positive in regions of upward motion such as the deep tropics and negative in regions of descending motion such as the subtropics. Temperature perturbations modulate this advection pattern to some degree; around 500 hPa there is an equatorial minimum in $\bar{w}q^{cc}$ that corresponds to the minimum in temperature increase (Figure 12a).

[52] In the lower troposphere, changes in q^{RH} (relative humidity) are small compared to those in q^{cc}, so that $\overrightarrow{\bar{v}}\nabla_p q^{cc}$ (Figure 13c) dominates the horizontal advection of specific humidity. The $\overrightarrow{\bar{v}}\nabla_p q^{cc}$ represents a drying effect in the subtropical lower troposphere as the mean winds blow equatorward. The signature of this term is also seen in

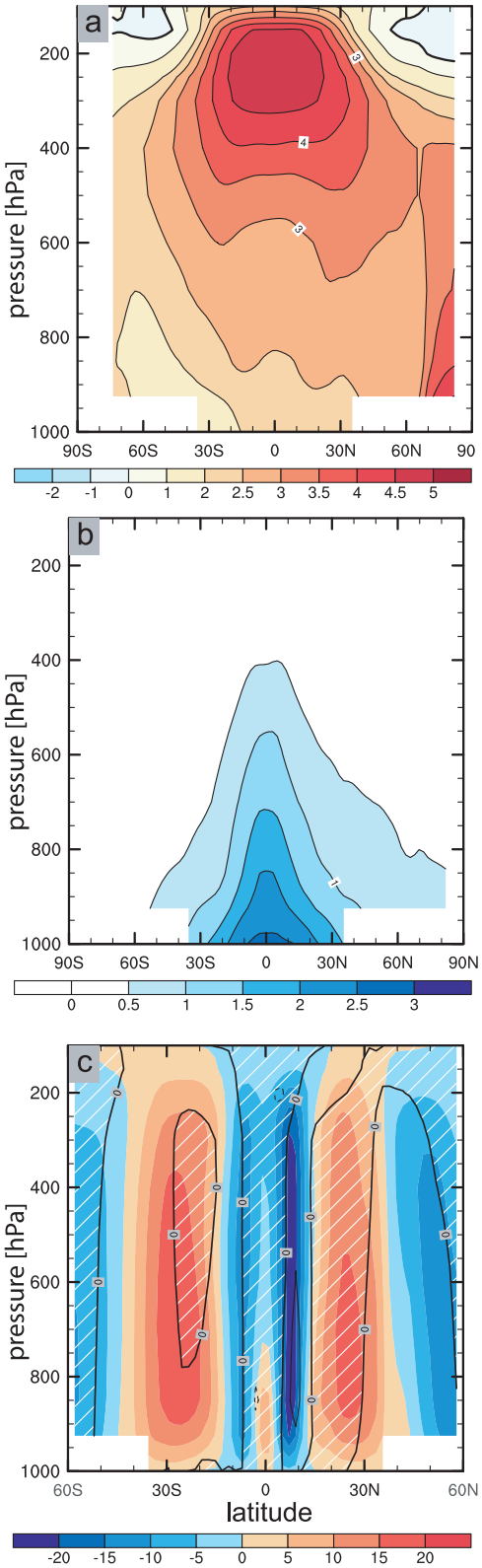

Figure 12. Latitude-height sections of zonal mean changes between 2000 and 2010 and 2090–2100 for (a) temperature (K), (b) specific humidity (g kg^{-1}), and (c) vertical pressure velocity (hPa d^{-1}, contours), with white crosshatching denoting negative values (anomalous upward motion). The shading in Figure 12c shows the mean vertical velocity (hPa d^{-1}) for the period 2000–2010.

the sum of all advection terms (Figure 13d). Its pronounced negative values in the off-equatorial lower troposphere contribute to the contrast between negative and positive advection tendencies in the subtropics and tropics, respectively (Figure 13d). The third horizontal advection term, $v'\nabla_p\bar{q}$, is small in comparison.

[53] Of the terms discussed above, $w'\partial\bar{q}/\partial p$ is more pronounced on the equator while $\bar{w}\partial q^{cc}/\partial p$ and horizontal advection dominate elsewhere. As a result, the sum of all terms (Figure 13d) is similar to $\bar{w}\partial q^{cc}/\partial p$, with its simple meridional structure that broadly resembles RH'. Specific humidity advection explains rather well the increase of relative humidity in the midtroposphere in 10°S–10°N and the negative values of RH' in the subtropical troposphere, but not the negative RH' in the tropical upper troposphere that results from the maximum in T'. Most importantly, the strong advective drying in the subtropical lower troposphere, cannot explain the relative humidity increase close to the surface. This discrepancy suggests subgrid vertical processes as the most likely cause of the surface relative humidity increase, although the AR4 archive does not allow a direct assessment of vertical mixing change. Near-surface atmospheric stability increases as evidenced by both SAT-SST and lower troposphere Richardson number changes (Figure 8). The increased stability helps trap moisture near the surface and thus contributes to the increase in surface relative humidity. Another contribution comes from the thermal inertia of the ocean, which slows down the increase in surface air temperature.

6. Summary and Discussion

6.1. Summary

[54] We have examined the response of surface evaporation in IPCC-AR4 models under the A1B scenario of greenhouse gas forcing for the 21st century. On average, the models simulate a rate of increase at ~2%/K, commensurate with the increase in precipitation reported in previous studies [*Held and Soden*, 2006]. This rate of increase is significantly lower than the 7%/K rate one might expect from the CC equation if the general circulation remained unchanged. While precipitation increases are concentrated in the equatorial region, evaporation increases have a broader meridional structure, with two subtropical peaks and an equatorial minimum.

[55] To explain the muted evaporation (and precipitation) response, we decompose latent heat flux into several terms representing distinct atmospheric adjustments and the oceanic response to warming. The results show that the following atmospheric adjustments are the most important in slowing down latent heat flux increase: for a 90-year period, (1) atmospheric stability as represented by the SAT-SST difference increases by 0.2 K; (2) surface relative humidity increases by about 1%, possibly as a result of increased atmospheric stability; and (3) surface wind speed decreases by 0.02 m/s (significantly more in the northern subtropics).

[56] Surface relative humidity is often assumed constant in global warming studies but our analysis reveals a robust increase of about 1% over a 90-year period and shows that

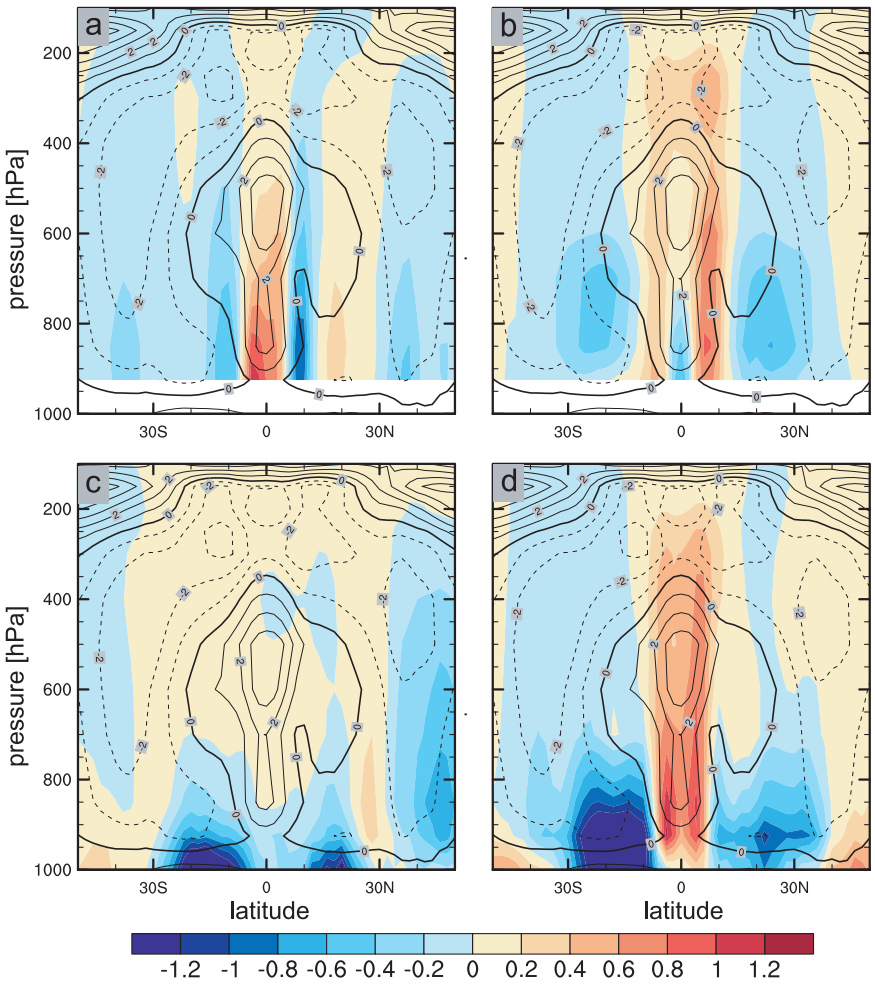

Figure 13. Zonal mean moisture advection terms (g kg^{-1} d^{-1} × 100; shading and white contours) for the model ensemble. Vertical pressure velocity (w) and horizontal velocity (v) are decomposed into two terms: $\bar{w}$ and w'. $\bar{w}$ is defined as the average over the period 2000–2010, while w' is the difference between the average over 2090–2100 and $\bar{w}$. Specific humidity, q, is decomposed into three terms: $\bar{q}$, q^{cc}, and q', where $\bar{q}$ is defined analogously to $\bar{w}$ (see text for more details). The following terms are plotted: (a) $w'\partial\bar{q}/\partial p$, (b) $\bar{w}\partial q^{cc}/\partial p$, (c) $\bar{\vec{v}}\,\nabla q^{cc}$, and (d) the sum of all terms. In each panel the change in relative humidity (%; black contour lines, negative contours dashed) between 2000 and 2100 is repeated for reference.

this constitutes an important climate feedback slowing down the surface evaporation increase. The increase in relative humidity is confined to a thin surface layer. Above this surface layer, we find a widespread decrease in the subtropics and midlatitudes and a midtropospheric increase centered over the equator, a pattern that seems related to the mean Hadley circulation: increases of about 5% in the ascending branch and decreases of about −3% in the descending branches. Three-dimensional moisture advection appears to explain the pattern of relative humidity changes in the free troposphere, but not in the surface layer where relative humidity increases despite advective drying. This leads us to suggest that increased surface stability exerts an important influence on surface relative humidity by trapping moisture near the surface.

[57] For the increase in surface relative humidity an analogy to advection fog can be drawn. The slow response of SST under global warming cools, or rather retards the warming of, the overlying air and thus increases relative humidity. This is, of course, only a partial analogy, as it is not advection but rather the different adjustment timescales of the atmosphere and underlying ocean that are responsible for the temperature difference.

6.2. Discussion

[58] The precipitation response to GHG forcing is far from horizontally uniform. The zonal mean precipitation changes, for example, are marked by a pronounced peak in the equatorial region. This equatorial peak is close to the CC rate of 7%/K but still below the increase in precipitable water, which also peaks on the equator. In the subtropics, on the other hand, precipitation decreases in all the models despite positive changes in precipitable water, consistent with the stabilization of the lower troposphere over the

subtropics. Thus changes in stability and circulation rather than in moisture dominate the precipitation response over the subtropical oceans.

[59] In view of the widespread relative humidity decrease in the subtropical free troposphere, it is surprising that relative humidity increases so consistently among models at the surface. Whether this shallow relative humidity increase simulated by the models is a realistic response to GHG forcing remains to be verified by observations. Studies by *Dai* [2006] and *Willett et al.* [2007] seem to suggest otherwise but, clearly, reliable data records are too short and the current warming too weak for a definitive answer. The small simulated changes in air-sea temperature difference, on the order of 0.025 K per decade, are also difficult to detect from observations. The globally averaged surface wind speed changes are even smaller, but there are some robust regional patterns of significant amplitude in the models, such as the intensification of the westerlies over the Southern Ocean, which is consistent with observations. Similarly, the robust intensification of the southeast trades, if realistic, might soon be detectable in observations. Furthermore, granted continued satellite observations, it should soon be possible to validate the very pronounced relative humidity increase in the midtroposphere ($\sim$0.5% per decade in the zonal mean).

[60] *Yu and Weller* [2007] employ a bulk formula approach in combination with observational data to estimate a trend in oceanic evaporation of 10% for the period 1981–2005, which corresponds to more than 30%/K. *Wentz et al.* [2007] analyze precipitation from the Special Sensor Microwave Imager (SSM/I) satellite instrument and find a trend of 7.0%/K for the period 1987–2006. They also estimate the trend in surface evaporation via bulk formula using SSM/I derived wind stress and other observations, which yields 6.9%/K. This close match with the precipitation trend might be fortuitous as their calculation rests on the assumption that surface relative humidity and air-sea temperature difference remain constant. Our analysis of model results suggests that, for a 1 K increase in surface temperatures, these quantities change by 0.35% and 0.05 K, respectively. Scaled to the 0.19 K increase of surface temperatures for the 19-year period analyzed by *Wentz et al.* [2007] these numbers become 0.07% and 0.01 K, which is clearly below the noise level of currently available data. Changes in relative humidity and air-sea temperature difference that are below the detection threshold could therefore produce evaporation estimates consistent with model simulations. Thus observational estimates of evaporation trends do not support the muted increase in simulations but, on the other hand, are clearly subject to large uncertainties and errors.

[61] The above considerations illustrate the need for long-term observations of surface relative humidity, SAT-SST difference, and surface wind speed, if we want to obtain reliable estimates of evaporation trends and, most of all, validate model simulations. Because the latent heat flux associated with evaporation changes is the major means for the ocean to balance radiative forcing [*Trenberth*, 1998], further ramifications on surface temperature might arise [*Du and Xie*, 2008]. Thus further studies of atmospheric feedback via surface heat flux, including sensitivity studies, are necessary to shed light on the dynamics of global warming and its consequences to the hydrological cycle.

Appendix A

A1. Details of the Latent Heat Flux Decomposition

[62] We begin by deriving expressions for the terms in the latent heat flux decomposition. To do this we form the partial derivative of the latent heat flux bulk formula with respect to each of its variables using (5). Considering only first-order derivatives this gives the following expression

$$Q'_E = \frac{\partial Q_E}{\partial T}T' + \frac{\partial Q_E}{\partial S}S' + \frac{\partial Q_E}{\partial RH}RH' + \frac{\partial Q_E}{\partial W}W' + \frac{\partial Q_E}{\partial \rho}\rho' + \frac{\partial Q_E}{\partial C_E}C'_E, \tag{A1}$$

where the individual terms are

$$\frac{\partial Q_E}{\partial T}T' = \frac{\alpha(b/T^2 - c/T) - RH\left(b/(T+S)^2 - c/(T+S)\right)}{\alpha - RH}Q_E T', \tag{A2}$$

$$\frac{\partial Q_E}{\partial \Delta T} = \frac{RH\left(b/(T+S)^2 - c/(T+S)\right)}{\alpha - RH}Q_E \Delta T', \tag{A3}$$

$$\frac{\partial Q_E}{\partial RH} = -\frac{Q_E}{\alpha - RH}RH', \tag{A4}$$

$$\frac{\partial Q_E}{\partial W}W' = \frac{Q_E}{W}W', \tag{A5}$$

where the terms represent the Newtonian cooling, air-sea temperature difference, relative humidity, and wind speed, in that order. Here α is defined as

$$\alpha \equiv \exp\left\{\frac{b}{T+S} - \frac{b}{T} - c\ln\left(\frac{T}{T+S}\right)\right\}.$$

The equations for the density and transfer coefficient (C_E) terms are analogous to (A5). A similar approach of latent heat flux decomposition was applied by *de Szoeke et al.* [2007] and *Du and Xie* [2008].

[63] The prime in equations (A2)–(A5) denotes the departure from monthly climatology, which, in our case, is based on the period 2046–2101. The use of a monthly climatology removes the seasonal cycle from the perturbations and helps keep the perturbations small compared to the mean. For the same reason, the decomposition is performed for each grid point separately.

[64] The density term in (A1) is on the order of -0.4 W m^{-2}. It is tightly controlled by surface air temperature and SST because surface pressure changes little under global warming. Therefore, it has been absorbed into the Newtonian cooling term, reducing it by $\sim$5%.

A2. Discussion of Possible Sources of Error in the Latent Heat Flux Decomposition

[65] One difficulty that arises in the computation of (A2)–(A5) is how to obtain Q_E. Calculating Q_E from model output via (1) is problematic because the exact form of the

Table A1. Cross Terms in the Latent Heat Flux Bulk Formula and Their Change Between the Periods 2046–2055 and 2091–2100[a]

	q_s		q_a		
	Term	Change	Term	Change	Σ
Monthly deviation of moisture × mean wind	$\hat{q}_s\bar{W}$	32.61	−27.87	4.74	$-\hat{q}_a\bar{W}$
Mean moisture × monthly deviation of wind	$\bar{q}_s\hat{W}$	−1.36	1.09	−0.27	$-\bar{q}_a\hat{W}$
Monthly deviation of moisture × monthly deviation of wind	$\hat{q}_s\hat{W}$	−0.42	0.34	−0.08	$-\hat{q}_a\hat{W}$
Daily deviation of moisture × daily deviation of wind	$q_s'W'$	0.00	0.11	0.11	$-q_a'W'$

[a]Unit is W m^{-2}; q_s, q_a, and W are surface saturation specific humidity, specific humidity, and wind speed, respectively. Bars, hats, and primes denote climatological mean, deviation of the monthly means from climatology, and deviation of the daily means from monthly means, respectively. Σ denotes the sum of the second and fourth column.

latent heat flux equation used is not available for all the models. Thus, instead of calculating Q_E from bulk formula, we use Q_E as output by the models. Q_E obtained in this way is likely to differ from what one would obtain by using (1) because of the nonlinearities inherent in both (1) and the actual model equations. For the climatological mean used here, the error is relatively small, but it certainly does contribute to the nonzero residuals seen in Figure 4.

[66] Another possible shortcoming of our calculations is the assumption of a constant transfer coefficient (C_E). The value of this quantity is not archived in the AR4 database so that possible trends can only be estimated. This proves difficult because the exact form of the bulk formula for each model is not known and because only time-averaged values of the input variables are available. As an alternative we calculated C_E from yearly averages using the *Fairall et al.* [1996] algorithm. This gives a negative contribution of approximately −0.1 W m^{-2}, consistent with the stabilization of the ocean-atmosphere interface but small compared to the other terms. Only an actual analysis of C_E calculated in the models can give a definite answer to whether this term is important or not. In view of the rather large unexplained residuals, the actual contribution from C_E likely exceeds our estimate.

[67] In the derivation of (A2)–(A5) we have expanded the bulk formula (1) by assuming small perturbations that are superimposed on the climatological mean cycle. Thus each of the equations (A2)–(A5) contains one perturbation variable multiplied by an expression that only contains mean variables. By construction, this rules out any contributions from cross correlation among variables and high-frequency variability, which might introduce a significant error in our calculations. We test this for one particular model, the GFDL CM 2.0, by writing (1) in the form

$$Q_E = \gamma(q_s - q_a)W, \tag{A6}$$

where $\gamma \equiv \rho_a L_v C_E$ is considered constant, while W, q_s, and q_a are decomposed according to $x = \bar{x} + \hat{x} + x'$. $\bar{x}$ is the climatological mean over the whole time series, $\hat{x}$ is the deviations of the monthly means from $\bar{x}$, and x' is the deviation of the daily means from $\hat{x}$. Applying this to all three variables and substituting into (A6) gives 18 terms. For these we calculate the difference between 2046 and 2055 and 2091–2100, and summarize the important contributions in Table A1. The $(\hat{q}_s - \hat{q}_a)\bar{W}$ dominates the balance: it is about 1 order of magnitude greater than the next largest contribution, $(\bar{q}_s - \bar{q}_a)\hat{W}$. The former term corresponds to the sum of Newtonian cooling, air-sea temperature difference and relative humidity contributions in Figure 4, while the latter corresponds to the wind speed contribution. The order-of-magnitude difference between the two is consistent with the very small wind speed term in the GFDL CM 2.0. The product of the monthly deviations, $(\hat{q}_s - \hat{q}_a)\hat{W}$, which is not accounted for in our decomposition, is about three times smaller than $(\bar{q}_s - \bar{q}_a)\hat{W}$. Given that the latter term is already rather unimportant, we conclude that cross terms only contribute a very moderate amount to the residual of the GFDL CM 2.0. Similar results are obtained for the other models.

Appendix B

[68] We decompose relative humidity changes into contributions from temperature (ΔRH_T) and specific humidity (ΔRH_q), by means of a Taylor expansion. First, using (4) and (6) we write relative humidity as

$$RH \equiv \frac{e}{e^*} = \frac{p/(1 - \varepsilon + \varepsilon/q)}{\exp(a - b/T - c\ln T)}, \tag{B1}$$

where e is vapor pressure, e^* saturation vapor pressure, q specific humidity, the ratio of the gas constants for dry air and water vapor, a, b, and c are constants whose values are given by *Emanuel* [1994], and other symbols have their conventional meanings. For temperatures below −10°C an equivalent form of (B1) with the saturation vapor pressure over ice is used. To calculate ΔRH_T and ΔRH_q we perform a Taylor expansion of (B1) in T and q using the first- and second-order derivatives.

[69] The relative humidity changes calculated as the sum of ΔRH_T and ΔRH_q are compared to the actual changes for the ensemble mean (Figure B1a). While the qualitative agreement is reasonable, it is obvious that the approximation cannot fully reproduce the actual changes, particularly in the upper troposphere. The major problem does not lie with the inaccuracy of the Taylor expansion, as the sum of ΔRH_T and ΔRH_q agrees very well with the total ΔRH calculated by substituting the temperature and moisture changes into (B1) (not shown). Rather it is the fact that the off-line relative humidity is calculated from monthly means, which cannot capture the nonlinearity of high-frequency fluctuations. Another possible reason is the presence of ice phase in the upper troposphere. Notwithstanding its shortcomings, the decomposition is good

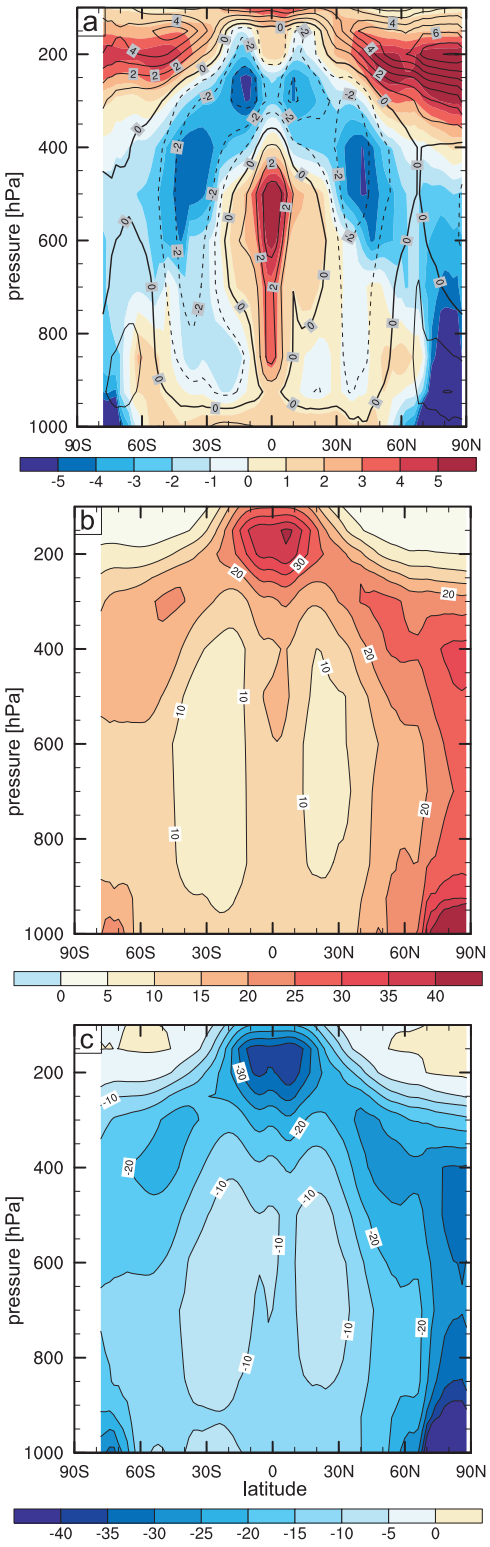

Figure B1. Analysis of the zonal mean relative humidity changes (%) between 2000 and 2100 for the model ensemble. (a) Actual relative humidity change (black contours; 1% interval) and the change derived from a Taylor expansion of the relative humidity equation with respect to temperature and specific humidity (color shading). (b and c) Relative humidity changes due to specific humidity changes and temperature changes, respectively. See text for more details.

enough to give a qualitative idea of the contributions from ΔRH_T and ΔRH_q.

[70] The zonal means of ΔRH_T and ΔRH_q are shown Figures B1b and B1c, respectively. ΔRH_q is positive everywhere consistent with the ubiquitous increase in specific humidity (Figure 12b). Values range from 0% in the upper troposphere over high latitudes to over 50% in the lower tropospheric arctic region and the upper tropospheric equatorial region. ΔRH_T, on the other hand, is negative everywhere with the exception of the extratropical upper troposphere. In the tropical lower troposphere and midtroposphere ΔRH_q dominates over ΔRH_T so that relative humidity increases. In the subtropics and midlatitudes, on the other hand, ΔRH_q is not large enough to completely balance ΔRH_T resulting in a decrease of relative humidity. In the upper troposphere, outside the tropics, ΔRH_T is small or even positive so that relative humidity increases.

[71] **Acknowledgments.** The authors would like to thank Yan Du for helpful discussions. Thanks also go to Jian Lu and two anonymous reviewers for their insightful comments. We also acknowledge the international modeling groups for providing their data for analysis and the Program for Climate Model Diagnosis and Intercomparison (PCMDI) for collecting and archiving the model data. The IPCC Data Archive at Lawrence Livermore National Laboratory is supported by the Office of Science, U.S. Department of Energy. This study was supported, in part, by National Oceanic and Atmospheric Administration grant NOAA NA17RJ1230 and by the Japanese Agency for Marine-Earth Science and Technology. IPRC publication 559. SOEST publication 7580.

References

Allan, R. P., and B. J. Soden (2007), Large discrepancy between observed and simulated precipitation trends in the ascending and descending branches of the tropical circulation, *Geophys. Res. Lett.*, *34*, L18705, doi:10.1029/2007GL031460.

Broecker, W. S. (1991), The great ocean conveyor, *Oceanography*, *4*, 79–89.

Cess, R. D., et al. (1990), Intercomparison and interpretation of climate feedback processes in 19 atmospheric general circulation models, *J. Geophys. Res.*, *95*, 16,601–16,615, doi:10.1029/JD095iD10p16601.

Chang, P., et al. (2006), Climate fluctuations of tropical coupled system—The role of ocean dynamics, *J. Clim.*, *19*, 5122–5174, doi:10.1175/JCLI3903.1.

Chou, C., and J. D. Neelin (2004), Mechanisms of global warming impacts on regional tropical precipitation, *J. Clim.*, *17*, 2688–2701, doi:10.1175/1520-0442(2004)017<2688:MOGWIO>2.0.CO;2.

Dai, A. (2006), Recent climatology, variability, and trends in global surface humidity, *J. Clim.*, *19*, 3589–3606, doi:10.1175/JCLI3816.1.

Deser, C., and A. S. Phillips (2008), Atmospheric circulation trends, 1950–2000: The relative roles of sea surface temperature forcing and direct atmospheric radiative forcing, *J. Clim.*, in press.

de Szoeke, S. P., S. P. Xie, T. Miyama, K. J. Richards, and R. J. O. Small (2007), What maintains the SST front north of the Eastern Pacific equatorial cold tongue?, *J. Clim.*, *20*, 2500–2514, doi:10.1175/JCLI4173.1.

Du, Y., and S.-P. Xie (2008), Role of atmospheric adjustments in the tropical Indian Ocean warming during the 20th century in climate models, *Geophys. Res. Lett.*, *35*, L08712, doi:10.1029/2008GL033631.

Emanuel, K. A. (1994), *Atmospheric Convection*, 580 pp., Oxford Univ. Press, New York.

Emori, S., and S. J. Brown (2005), Dynamic and thermodynamic changes in mean and extreme precipitation under changed climate, *Geophys. Res. Lett.*, *32*, L17706, doi:10.1029/2005GL023272.

Fairall, C. W., E. F. Bradley, D. P. Rogers, J. B. Edson, and G. S. Young (1996), Bulk parameterization of air-sea fluxes for TOGA COARE, *J. Geophys. Res.*, *101*, 3747–3767, doi:10.1029/95JC03205.

Fyfe, J. C., and O. A. Saenko (2005), Human-induced change in the Antarctic Circumpolar Current, *J. Clim.*, *18*, 3068–3073, doi:10.1175/JCLI3447.1.

Gillett, N. P., and D. W. J. Thompson (2003), Simulation of recent Southern Hemisphere climate change, *Science*, *302*, 273–275, doi:10.1126/science.1087440.

Gordon, H. B., et al. (2002), The CSIRO Mk3 Climate System Model, *CSIRO Atmos. Res. Tech. Pap. 60*, 130 pp., Commonw. Sci. and Ind. Res. Org., Aspendale, Victoria, Australia.

Gregory, J. M. (2000), Vertical heat transports in the ocean and their effect on time-dependent climate change, *Clim. Dyn.*, *16*, 501–515, doi:10.1007/s003820000059.

Held, I. M., and B. J. Soden (2000), Water vapor feedback and global warming, *Annu. Rev. Energy Environ.*, *25*, 441–475, doi:10.1146/annurev.energy.25.1.441.

Held, I. M., and B. J. Soden (2006), Robust responses of the hydrological cycle to global warming, *J. Clim.*, *19*, 5686–5699, doi:10.1175/JCLI3990.1.

Ingram, W. J. (2002), On the robustness of the water vapor feedback: GCM vertical resolution and formulation, *J. Clim.*, *15*, 917–921, doi:10.1175/1520-0442(2002)015<0917:OTROTW>2.0.CO;2.

Kushner, P. J., I. M. Held, and T. L. Delworth (2001), Southern Hemisphere atmospheric circulation response to global warming, *J. Clim.*, *14*, 2238–2249, doi:10.1175/1520-0442(2001)014<0001:SHACRT>2.0.CO;2.

Lambert, F. H., A. R. Stine, N. Y. Krakauer, and J. C. H. Chiang (2008), How much will precipitation increase with global warming?, *Eos Trans. AGU*, *89*, 193–194, doi:10.1029/2008EO210001.

Levitus, S., J. Antonov, and T. Boyer (2005), Warming of the world ocean, 1955–2003, *Geophys. Res. Lett.*, *32*, L02604, doi:10.1029/2004GL021592.

Louis, J.-F. (1979), A parametric model of vertical eddy fluxes in the atmosphere, *Boundary Layer Meteorol.*, *17*, 187–202, doi:10.1007/BF00117978.

Lu, J., G. A. Vecchi, and T. Reichler (2007), Expansion of the Hadley cell under global warming, *Geophys. Res. Lett.*, *34*, L06805, doi:10.1029/2006GL028443.

Peixoto, J. P., and A. H. Oort (1996), The climatology of relative humidity in the atmosphere, *J. Clim.*, *9*, 3443–3463, doi:10.1175/1520-0442(1996)009<3443:TCORHI>2.0.CO;2.

Pierrehumbert, R. (1995), Thermostats, radiator fins, and the local runaway greenhouse, *J. Atmos. Sci.*, *52*, 1784–1806, doi:10.1175/1520-0469(1995)052<1784:TRFATL>2.0.CO;2.

Previdi, M., and B. G. Liepert (2008), Interdecadal variability of rainfall on a warming planet, *Eos Trans. AGU*, *89*, 193, 195.

Sandor, B., E. Jensen, E. Stone, W. Read, J. Waters, and J. Mergenthaler (2000), Upper tropospheric humidity and thin cirrus, *Geophys. Res. Lett.*, *27*, 2645–2648, doi:10.1029/1999GL011194.

Santer, B. D., et al. (2003), Contributions of anthropogenic and natural forcing to recent tropopause height changes, *Science*, *301*, 479–483, doi:10.1126/science.1084123.

Santer, B. D., et al. (2005), Amplification of surface temperature trends and variability in the tropical atmosphere, *Science*, *309*, 1551–1556, doi:10.1126/science.1114867.

Sherwood, S. C., E. R. Kursinski, and W. G. Read (2006), A distribution law for free-tropospheric relative humidity, *J. Clim.*, *19*, 6267–6277.

Smith, R. N. B. (1990), A scheme for predicting layer clouds and their water content in a general circulation model, *Q. J. R. Meteorol. Soc.*, *116*, 435–460, doi:10.1002/qj.49711649210.

Soden, B. J., and F. P. Bretherton (1993), Upper troposphere relative humidity from the GOES 6.7 μm channel: Method and climatology for July 1987, *J. Geophys. Res.*, *98*, 16,669–16,688, doi:10.1029/93JD01283.

Soden, B. J., D. L. Jackson, V. Ramaswamy, M. D. Schwarzkopf, and X. L. Huang (2005), The radiative signature of upper tropospheric moistening, *Science*, *310*, 841–844, doi:10.1126/science.1115602.

Spencer, R. W., and W. D. Braswell (1997), How dry is the tropical free troposphere? Implications for global warming theory, *Bull. Am. Meteorol. Soc.*, *78*, 1097–1106, doi:10.1175/1520-0477(1997)078<1097:HDITTF>2.0.CO;2.

Thompson, D. W. J., and S. Solomon (2002), Interpretation of recent Southern Hemisphere climate change, *Science*, *296*, 895–899, doi:10.1126/science.1069270.

Trenberth, K. E. (1998), Atmospheric moisture residence times and cycling: Implications for rainfall rates and climate change, *Clim. Change*, *39*, 667–694, doi:10.1023/A:1005319109110.

Trenberth, K. E., A. Dai, R. M. Rasmussen, and D. B. Parsons (2003), The changing character of precipitation, *Bull. Am. Meteorol. Soc.*, *84*, 1205–1217.

Trenberth, K. E., J. Fasullo, and L. Smith (2005), Trends and variability in column-integrated water vapor, *Clim. Dyn.*, *24*, 741–758.

Vecchi, G. A., and B. J. Soden (2007), Global warming and the weakening of the tropical circulation, *J. Clim.*, *20*, 4316–4340, doi:10.1175/JCLI4258.1.

Wentz, F. J., and M. Schabel (2000), Precise climate monitoring using complementary satellite data sets, *Nature*, *403*, 414–416, doi:10.1038/35000184.

Wentz, F. J., L. Ricciardulli, K. Hilburn, and C. Mears (2007), How much more rain will global warming bring?, *Science*, *317*, 233–235, doi:10.1126/science.1140746.

Willett, K. M., N. P. Gillet, P. D. Jones, and P. W. Thorne (2007), Attribution of observed surface humidity changes to human influence, *Nature*, *449*, 710–713, doi:10.1038/nature06207.

Xie, S.-P. (2004), The shape of continents, air-sea interaction, and the rising branch of the Hadley circulation, in *The Hadley Circulation: Past, Present and Future*, edited by H. F. Diaz and R. S. Bradley, pp. 121–152, Kluwer Acad., Dordrecht, Netherlands.

Xu, K.-M., and K. A. Emanuel (1989), Is the tropical atmosphere conditionally unstable?, *Mon. Weather Rev.*, *117*, 1471–1479, doi:10.1175/1520-0493(1989)117<1471:ITTACU>2.0.CO;2.

Yang, X. Y., R. X. Huang, and D. X. Wang (2007), Decadal changes of wind stress over the Southern Ocean associated with Antarctic ozone depletion, *J. Clim.*, *20*, 3395–3410, doi:10.1175/JCLI4195.1.

Yin, J. H. (2005), A consistent poleward shift of the storm tracks in simulations of 21st century climate, *Geophys. Res. Lett.*, *32*, L18701, doi:10.1029/2005GL023684.

Yu, L., and R. A. Weller (2007), Objectively analyzed air–sea heat fluxes for the global ice-free oceans (1981–2005), *Bull. Am. Meteorol. Soc.*, *88*, 527–539, doi:10.1175/BAMS-88-4-527.

I. Richter and S.-P. Xie, International Pacific Research Center, SOEST, University of Hawaii at Manoa, Honolulu, HI 96822, USA. (irichter@hawaii.edu)